

CLASSICAL DYNAMICS OF A THIN MOVING MIRROR AND A SINGLE-MODE FIELD

L. O. Castaños* and R. Weder⁺

*Departamento de Física Matemática, Instituto de Investigaciones en Matemáticas Aplicadas y en Sistemas,
Universidad Nacional Autónoma de México, Apartado Postal 20-726, México DF 01000, México*

We analyze the classical dynamics of a system composed of a one-dimensional cavity with a perfect fixed mirror and a movable mirror with non-zero transparency interacting with a single-mode electromagnetic field by means of radiation pressure. The movable mirror is assumed to be thin so that it is modelled by a delta function and we use the exact modes of the complete system. The transparency and the mirror-position dependent cavity resonance frequencies are built into the modes and this allows us to deduce that the radiation pressure force comes from a periodic potential with period half the wavelength of the field. The exact modes and the radiation pressure potential allow us to give intuitive physical interpretations of the dynamics of the system and to obtain approximate analytic solutions for the motion of the mirror. Three regimes are identified depending on the intensity of the field and it is found that the dynamics can be qualitatively very different in each of them with some regimes being very sensitive to the values of the parameters. Moreover, we determine conditions when the Maxwell-Newton equations used to describe the system constitute accurate approximations of the exact equations governing the dynamics.

PACS numbers: 42.50.Wk, 42.65.-k, 05.45.-a

I. INTRODUCTION

The area of optomechanics has received much attention due to potential applications ranging from precision measurements to fundamental tests of quantum mechanics to optical communications [1–3]. Optomechanical systems not only have the potential to become a powerful probe with which to explore the quantum world [2, 4–10], but are also of great interest in the area of optical micro-electromechanical systems [3] and constitute a setting in which classical non-linear dynamics have to be analyzed [11–19].

One of the paradigmatic models in optomechanics consists of a cavity with one movable mirror. The movable mirror is a mechanical oscillator and it is coupled to the electromagnetic field by radiation pressure and by thermal or bolometric effects (absorption of photons distorting and displacing the mirror). The classical dynamics of this type of systems have been studied in [11–19]. For the quantum dynamics we refer the reader to [1, 2, 4–10].

The classical dynamics of an optomechanical set-up similar to the model described above and dominated by bolometric forces have been studied both experimentally and theoretically [13, 14]. It was found that self-sustained oscillations of the movable mirror are present, that their amplitude settles into one of several attractors (see also [19] for this phenomenon), and that there is a regime where two mechanical modes of oscillation can be excited. Moreover, it was suggested that the multi-stability can be used as a device to measure small displacements.

The classical dynamics of a set-up dominated by radiation pressure has also been studied both experimentally and theoretically [11, 12]. It is composed of a toroid cavity and a pump beam. The toroid cavity executes a periodic motion that was explained by the following intuitive physical picture: radiation pressure induces a

flex of the cavity that takes it out of resonance with the pump beam; this leads to a reduction of radiation pressure and, as a consequence, the cavity moves back into resonance and the process starts over again. It was found that the cavity vibrations cause modulation of the input pump beam and that this modulation becomes random oscillations with sufficiently high pump power [11]. Moreover, a radiation pressure induced parametric oscillation instability (a regenerative oscillation of mechanical eigenmodes) was analyzed [12].

The case where both radiation pressure and thermal effects are relevant has also been studied [15–18]. It has been shown experimentally and theoretically [15, 16] that these two types of forces operate at different time scales and can lead to dynamics in which chaotic attractors appear. Also, [17] established a very detailed phenomenological model for a micromechanical mirror that incorporates non-linear elastic and dissipative terms, an external excitation force as well as the radiation pressure and thermal forces. The model was used to describe the results of an experimental study of the dynamics of an optomechanical cavity with micro-mechanical mirrors in two different geometries [18].

In this article we investigate the classical dynamics of a thin cavity movable mirror modelled by a delta-function interacting with a classical single-mode electromagnetic field by means of radiation pressure. Our approach differs from most articles in that we start from approximate Maxwell-Newton equations valid when the velocity and acceleration of the movable mirror is small and we consider the exact modes of the complete system, that is, we do not divide them into modes of the cavity and modes outside of it as if the cavity were composed of perfect mirrors and then couple them through a phenomenological interaction [28]. This allows us to incorporate both the transparency of the mirror and the mirror-position

dependent cavity resonance frequencies directly in the modes.

As a result of our treatment, we derive the radiation pressure force from a periodic potential and the physical process governing the dynamics in the case of the toroid cavity mentioned above is explicitly and rigorously derived from our equations. The radiation pressure potential gives physical insight into the dynamics of the system and allows us to determine approximate analytical solutions for the motion of the movable mirror. Also, special attention is paid in establishing the conditions under which the model is valid. The intention is to shed more light into the physics and the intricate dynamics of the movable mirror-electromagnetic field system as well as to have a more profound understanding of when the approximate Maxwell-Newton equations normally used to describe this type of systems are valid.

The model of a *fixed very thin mirror* with non-zero transparency modelled by a delta-function (known as the Lang-Scully-Lamb or LSL model) has been used in the past [20–27]. Originally it was introduced as a simple more realistic model of a laser with the purpose to explain physical phenomena that could not be answered (at least satisfactorily) with the phenomenological models. In particular, it was used to explain why the laser line is so narrow, to form a better conceptual picture of the nature of a laser mode, and to account for radiation losses through one of the mirrors of the laser without the use of phenomenological models [20–22, 28]. The investigations were initially restricted to semi-classical treatments and were later extended to full quantum treatments [23–25]. Afterwards, the same model was used to explain why the phenomenological models work in the good cavity limit [26] and to deduce a master equation to incorporate the effects of a finite mirror transmissivity [27].

The article is organized as follows. In Section II we establish the system under study and the model used to describe it. In Section III we restrict to a single-mode field and derive the potential associated with the radiation pressure force. In Section IV we investigate the dynamics of the movable mirror. In Sections V and VI we consider the cases where the movable mirror is also subject to friction and to a harmonic oscillator potential. Finally, the conclusions are given in Section VII.

II. THE MODEL

Consider a one-dimensional cavity composed of a fixed and perfect (zero transparency) mirror and a movable mirror, both parallel to the yz -plane. The fixed mirror is located at $x = 0$, while the movable mirror is located at $x = q(t) > 0$ at time t and has thickness δ_{thick} when it is at rest. We assume that the movable mirror is a linear, isotropic, homogeneous, non-magnetizable, and non-conducting (it does not contain any free charges or currents) dielectric when it is at rest. For the electromagnetic field we shall use the Gaussian system of units. We

also assume that the electric field is polarized along the z -axis. This allows us to take the scalar potential equal to zero and to derive both the electric and magnetic fields from a vector potential. Explicitly, the vector potential $\mathbf{A}(x, t)$ is of the form

$$\mathbf{A}(x, t) = A_0(x, t)\mathbf{z}, \quad (1)$$

while the electric $\mathbf{E}(x, t)$ and magnetic $\mathbf{B}(x, t)$ fields are given by

$$\begin{aligned} \mathbf{E}(x, t) &= -\frac{1}{c} \frac{\partial A_0}{\partial t}(x, t)\mathbf{z}, \\ \mathbf{B}(x, t) &= -\frac{\partial A_0}{\partial x}(x, t)\mathbf{y}. \end{aligned} \quad (2)$$

Notice that we are working in the Coulomb gauge.

The equation for the vector potential is given by

$$\frac{\partial^2 A_0}{\partial x^2}(x, t) = \frac{\epsilon[x - q(t)]}{c^2} \frac{\partial^2 A_0}{\partial t^2}(x, t), \quad (3)$$

for all $x > 0$ and $t \in \mathbb{R}$. Here ϵ is the dielectric function associated with the movable mirror.

In order to take into account the perfect and fixed mirror at $x = 0$ one needs to impose the following boundary condition:

$$\frac{\partial A_0}{\partial t}(0+, t) = 0 \quad (t \in \mathbb{R}). \quad (4)$$

This condition comes from imposing $\mathbf{E}(x, t) = \mathbf{B}(x, t) = \mathbf{0}$ for $x < 0$ and using the usual boundary conditions for the electromagnetic field.

In reference [29] it is shown that (3) is obtained by posing Maxwell's equations in inertial reference frames in which the movable mirror is instantaneously at rest and then changing back to the laboratory reference frame (defined by the condition that the perfect mirror is fixed at $x = 0$) using (instantaneous) Lorentz transformations and neglecting terms of order $\dot{q}(t)/c$, $\ddot{q}(t)/(c\omega_0)$, and second powers of them. Here c is the speed of light in vacuum and ω_0 is the characteristic frequency of the electromagnetic field. Hence, (3) will be an accurate approximation to the exact equation governing the dynamics of $A_0(x, t)$ if the following two conditions are satisfied:

$$\left| \frac{\dot{q}(t)}{c} \right|, \left| \frac{\ddot{q}(t)}{c\omega_0} \right| \ll 1 \quad (t \in \mathbb{R}). \quad (5)$$

In reference [29] it is shown that equations (3) and (4) are valid for general dielectric functions $\epsilon[x - q(t)]$. In the rest of the article we assume that the movable mirror is very thin, that is

$$\delta_{\text{thick}} \ll \lambda \equiv \frac{2\pi c}{\omega_0}. \quad (6)$$

Hence, one can approximate the dielectric function associated with the movable mirror by a delta function:

$$\epsilon[x - q(t)] = 1 + 4\pi\chi_0\delta[x - q(t)]. \quad (7)$$

Here χ_0 has units of length. In [29] we prove that (3) is valid with $\epsilon[x - q(t)]$ given in (7) by a limiting process starting with regular $\epsilon[x - q(t)]$. Notice that (3) and (4) with (7) correspond to the LSL model discussed in the Introduction but now with a moving mirror.

Using the law of conservation of linear momentum for the system (electromagnetic field + dielectric mirror at $x = q(t)$ + fixed perfect mirror at $x = 0$) it follows from (3) and (7) that the equation for the movable mirror is given by [29]

$$M_0 \ddot{q}(t) = -\frac{1}{8\pi} \left\{ \left[\frac{\partial A_0}{\partial x} [q(t)+, t] \right]^2 - \left[\frac{\partial A_0}{\partial x} [q(t)-, t] \right]^2 \right\}, \quad (8)$$

for all $t \in \mathbb{R}$. Here M_0 has units of mass per unit area and

$$\frac{\partial A_0}{\partial x} [q(t) \pm, t] = \lim_{x \rightarrow q(t) \pm} \frac{\partial A_0}{\partial x} (x, t). \quad (9)$$

Note that (3) corresponds to the usual wave-equation for the potential with the mirror instantaneously fixed at $q(t)$. Moreover, the right-hand side of (8) is the radiation pressure exerted by the electromagnetic field on the mirror instantaneously fixed at $q(t)$. These equations are accurate approximations when (5) are valid, since they imply that the movable mirror has both a velocity and an acceleration sufficiently small so that the field evolves as if the movable mirror were instantaneously fixed at its position $q(t)$. In other words, the field *sees* the movable mirror as if it were fixed at $q(t)$.

We now proceed to solve (3) and (8). In order to do this we first introduce the modes of the system for fixed $q(t)$.

A. Modes for fixed $q(t)$

For $q(t)$ fixed, the modes associated with (3), (4), and (7) were calculated in [22]. Adapting them to our coordinate system one finds that they are given by

$$V_k[x, q(t)] = \begin{cases} L_k[q(t)] \sin(kx) & \text{if } 0 \leq x \leq q(t), \\ \sqrt{\frac{2}{\pi}} \sin \{k[x - q(t)] + \delta_k[q(t)]\} & \text{if } x > q(t). \end{cases} \quad (10)$$

Here $k > 0$ and

$$L_k[q(t)] = \sqrt{\frac{2}{\pi}} \left\{ 1 + (4\pi\chi_0 k)^2 \sin^2[kq(t)] - (4\pi\chi_0 k) \sin[2kq(t)] \right\}^{-1/2},$$

$$\sin \{\delta_k[q(t)]\} = \sqrt{\frac{\pi}{2}} L_k[q(t)] \sin[kq(t)],$$

$$\cos \{\delta_k[q(t)]\} = \sqrt{\frac{\pi}{2}} L_k[q(t)] \times \left\{ \cos[kq(t)] - (4\pi\chi_0 k) \sin[kq(t)] \right\}. \quad (11)$$

For fixed k the transmissivity T of the movable mirror is given by [22]

$$T = \left[1 + \left(\frac{4\pi\chi_0 k}{2} \right)^2 \right]^{-1}. \quad (12)$$

Hence, the transparency of the movable mirror will be small if $T \ll 1$ or, equivalently, $4\pi\chi_0 k \gg 1$.

Before proceeding we give some properties of $L_k[q(t)]$ that are deduced in Appendix I. The function $L_k[q(t)]$ is maximized (minimized) for a discrete set of values q_{2n} (q_{2n+1}) of $q(t)$ with $n \in \mathbb{Z}^+$. Here \mathbb{Z}^+ is the set of non-negative integers. If $4\pi\chi_0 k \gtrsim 5$, then one has to good approximation

$$\begin{aligned} kq_{2n} &\simeq n\pi + \frac{1}{4\pi\chi_0 k}, \\ kq_{2n+1} &\simeq \left(n + \frac{1}{2}\right)\pi + \frac{1}{4\pi\chi_0 k}, \end{aligned} \quad (13)$$

and

$$\begin{aligned} L_k(q_{2n}) &\simeq \sqrt{\frac{2}{\pi}} (4\pi\chi_0 k), \\ L_k(q_{2n+1}) &\simeq \sqrt{\frac{2}{\pi}} \left(\frac{1}{4\pi\chi_0 k} \right). \end{aligned} \quad (14)$$

Notice that $kq_{2n} \rightarrow n\pi$ as $4\pi\chi_0 k \rightarrow +\infty$, that is, q_{2n} tends to the values $n\pi/k$ corresponding to the case where the movable mirror is perfect [30] as the transparency tends to zero.

Also, one can approximate $L_k(q)^2$ by a Lorentzian if the transparency of the movable mirror is small and one restricts q to an interval around q_{2n} whose endpoints are not near the minimizers $q_{2n \pm 1}$. Explicitly,

$$L_k(q)^2 \simeq \left(\frac{2}{\pi\xi^2} \right) \frac{1}{k^2(q - q_{2n})^2 + \frac{1}{\xi^4}}, \quad (15)$$

with $\xi = 4\pi\chi_0 k$ if $k|q - q_{2n}| \ll 3/2$ and $2/\xi \ll 1$.

We now discuss the behavior of $L_k[q(t)]$ and its relation to the cavity resonance frequencies in the case where the transparency of the movable mirror is small, that is, in the case $4\pi\chi_0 k \gg 1$. Assume that $k > 0$ is fixed. As the mirror moves, $L_k[q(t)]$ will be very large only when $q(t) \simeq q_{2n}$ for some $n \in \mathbb{Z}^+$, see (14) and (15). As a result, $\omega = ck$ will coincide with one of the cavity resonance frequencies only when the mirror is sufficiently close to one of these special positions. In fact, from (15) it follows that $\omega = ck$ coincides with one of the cavity resonance frequencies if and only if $k|q - q_{2n}| \leq (4\pi\chi_0 k)^{-2}$. In other words, the resonant positions kq_{2n} have a half-width-at-half-maximum equal to $(4\pi\chi_0 k)^{-2}$. Figure 1

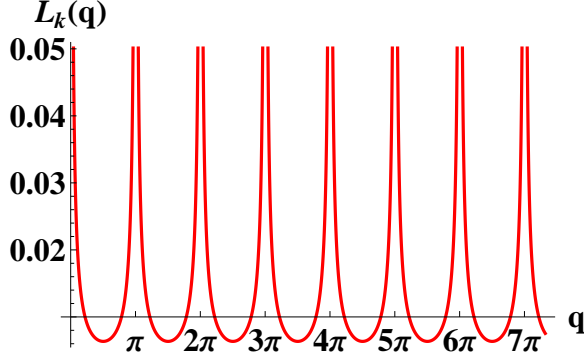


FIG. 1: (Color online) The figure illustrates $L_k(q)$ as a function of q for $\chi_0 = 10$ m and $k = 1$ m $^{-1}$. For a better illustration only part of the y -axis is shown.

shows $L_k(q)$ as a function of q for $\chi_0 = 10$ m and $k = 1$ m $^{-1}$.

The modes (10) form a continuous set which satisfies the following orthonormalization condition [22]:

$$\delta(k - k') = \int_0^{+\infty} dx \epsilon[x - q(t)] V_k[x, q(t)] V_{k'}[x, q(t)] . \quad (16)$$

Moreover, any function $f(x) \in \mathcal{L}^2[0, +\infty)$ can be expanded in the form [22]

$$f(x) = \int_0^{+\infty} dk f_k[q(t)] V_k[x, q(t)] , \quad (17)$$

with the k th-mode $f_k[q(t)]$ given by

$$f_k[q(t)] = \int_0^{+\infty} dx \epsilon[x - q(t)] V_k[x, q(t)] f(x) . \quad (18)$$

Using (17) and (18) it follows that

$$A_0(x, t) = \int_0^{+\infty} dk Q_k[t, q(t)] V_k[x, q(t)] , \quad (19)$$

with

$$Q_k[t, q(t)] = \int_0^{+\infty} dx \epsilon[x - q(t)] V_k[x, q(t)] A_0(x, t) . \quad (20)$$

Substituting (19) into (3), neglecting terms proportional to $\dot{q}(t)/c$, $[\dot{q}(t)/c]^2$, and $\ddot{q}(t)/(c\omega_0)$ (ω_0 the characteristic frequency of the field), and using the orthonormalization relation in (16) one obtains harmonic oscillator equations for each of the modes $Q_k[t, q(t)]$:

$$0 = \frac{d^2}{dt^2} Q_k[t, q(t)] + \omega_k^2 Q_k[t, q(t)] , \quad (21)$$

with $\omega_k = ck$, $k > 0$, and $t \in \mathbb{R}$. We have dropped terms proportional to $\dot{q}(t)/c$, $[\dot{q}(t)/c]^2$, and $\ddot{q}(t)/(c\omega_0)$ because

terms of these orders were neglected to obtain (3). Also notice that only by dropping these terms does one recover the physical situation described by (3) in which the field evolves as if the movable mirror were fixed.

From (21) one immediately obtains for $k > 0$ and $t \in \mathbb{R}$ that

$$Q_k[t, q(t)] = g(k)e^{-i\omega_k t} + g(k)^* e^{i\omega_k t} . \quad (22)$$

Here we used the fact that $Q_k[t, q(t)]$ must be a real quantity because $A_0(x, t)$ and $V_k[x, q(t)]$ are real.

III. SINGLE-MODE FIELD

In the rest of the article we assume that the field has a single-mode, that is,

$$g(k) = g_0 e^{i\phi_0} \delta(k - k_N^0) , \quad (23)$$

with $k_N^0, g_0 > 0$ and $\phi_0 \in \mathbb{R}$. We now discuss which physical situation is described approximately by (23). A single-mode laser on the far right is turned on. The travelling wave associated with the laser is partially reflected by the movable mirror at $q(t)$ and completely reflected by the perfect mirror fixed at $x = 0$. As a result a standing wave is (approximately) formed. This standing wave is defined by the mode in (10) with $k = k_N^0$. Moreover, it is exerting radiation pressure on the movable mirror and at the same time it is driving the electromagnetic field inside the cavity.

Substituting (22) and (23) in (19) it follows that

$$A_0(x, t) = 2g_0 \cos(\omega_0 t - \phi_0) V_{k_N^0}[x, q(t)] , \quad (24)$$

with $\omega_0 \equiv \omega_{k_N^0} = ck_N^0$. Notice that ϕ_0 represents the phase of $A_0(x, t)$ at time $t = 0$. In all that follows we choose an origin of time so that $\phi_0 = 0$ (this corresponds to making the time translation $t + \phi_0/\omega_0$).

All that remains is to solve equation (8) for the moving mirror. We first express (8) in terms of non-dimensional quantities.

Define

$$\begin{aligned} \Delta &= \sqrt{\frac{g_0^2 \omega_0^3}{\pi^2 M_0 c^3}} , \\ \xi &= 4\pi \chi_0 k_N^0 , \\ \Omega &= 2 \frac{\omega_0}{\Delta} , \\ x(\tau) &= k_N^0 q \left(\frac{\tau}{\Delta} \right) . \end{aligned} \quad (25)$$

Here Δ has units of 1/s, $\tau = \Delta t$ is the non-dimensional time, and ξ , Ω , and $x(\tau)$ are non-dimensional quantities. Notice that we have taken $1/k_N^0$ to be the characteristic length of the system, while $1/\Delta$ is the characteristic time. Also, from (12) and (25) it follows that the transmissivity

T of the movable mirror is given by

$$T = \left[1 + \left(\frac{\xi}{2} \right)^2 \right]^{-1}, \quad (26)$$

so that the transparency will be small if ξ is large.

Using (24) and (25) it can be shown that (8) can be rewritten as follows:

$$\frac{d^2 x}{d\tau^2}(\tau) = [1 + \cos(\Omega\tau)] f_{\text{RWA}}[x(\tau)], \quad (27)$$

with

$$f_{\text{RWA}}(x) = -\frac{1}{2} \left[1 - \frac{1}{1 + \xi^2 \sin^2(x) - \xi \sin(2x)} \right]. \quad (28)$$

Note that $1 + \xi^2 \sin^2(x) - \xi \sin(2x) > 0$ for all $x \in \mathbb{R}$. The notation $f_{\text{RWA}}(x)$ has been chosen because the term on the right of (27) will reduce to $f_{\text{RWA}}[x(\tau)]$ in the rotating wave approximation (RWA).

In this article derivatives with respect to τ are also denoted by a prime, while derivatives with respect to t are denoted by a dot.

The non-dimensional force on the right of (27) can be derived from the non-dimensional position and time dependent potential

$$V(x, t) = [1 + \cos(\Omega\tau)] V_{\text{RWA}}(x), \quad (29)$$

that is,

$$\begin{aligned} [1 + \cos(\Omega\tau)] f_{\text{RWA}}(x) &= -\frac{d}{dx} V(x, t), \\ f_{\text{RWA}}(x) &= -\frac{d}{dx} V_{\text{RWA}}(x). \end{aligned} \quad (30)$$

If $(2m-1)\pi/2 \leq x \leq (2m+1)\pi/2$ and $x \geq 0$ with $m \in \mathbb{Z}^+$, then $V_{\text{RWA}}(x)$ is given by

$$\begin{aligned} V_{\text{RWA}}(x) &= \frac{x}{2} - \frac{1}{2} \tan^{-1} [(1 + \xi^2) \tan(x) - \xi] \\ &\quad - \frac{1}{2} [\tan^{-1}(\xi) + m\pi]. \end{aligned} \quad (31)$$

The expression for $V_{\text{RWA}}(x)$ was obtained by integrating (28) from $x' = 0$ to $x' = x > 0$. Also, $\tan^{-1}\theta \in (-\pi/2, \pi/2)$ for $\theta \in \mathbb{R}$.

We now list properties of $V_{\text{RWA}}(x)$ and $f_{\text{RWA}}(x)$ that will be used throughout the article. They are deduced in Appendix II. Also, figure 2a illustrates $V_{\text{RWA}}(x)$ for $\xi = 1, 10$, and 50 .

1. Periodicity of $V_{\text{RWA}}(x)$: $V_{\text{RWA}}(x)$ is a periodic function of period π . This follows from the piecewise definition of $V_{\text{RWA}}(x)$ on intervals of length π and the fact that $\tan(x)$ is periodic of period π .
2. Maximizers of $V_{\text{RWA}}(x)$: They are denoted by x_n^* with $n \in \mathbb{Z}^+$. One has

$$x_n^* = n\pi, \quad V_{\text{RWA}}(x_n^*) = 0. \quad (32)$$

Also, 0 is the absolute maximum value of $V_{\text{RWA}}(x)$.

3. Minimizers of $V_{\text{RWA}}(x)$: They are denoted by x_n^{**} with $n \in \mathbb{Z}^+$. For $\xi \gtrsim 5$ and $n \in \mathbb{Z}^+$ one has to good approximation

$$\begin{aligned} x_n^{**} &\simeq n\pi + 2/\xi, \\ V_{\text{RWA}}(x_n^{**}) &\simeq V_{\text{RWA}}(2/\xi) \simeq -\tan^{-1}(\xi). \end{aligned} \quad (33)$$

Also, $V_{\text{RWA}}(x_n^{**})$ is the absolute minimum value of $V_{\text{RWA}}(x)$.

4. Bounds of $V_{\text{RWA}}(x)$: For all $x \geq 0$ one has

$$-\frac{\pi}{2} < V_{\text{RWA}}(x) \leq 0. \quad (34)$$

Also, $V_{\text{RWA}}(2/\xi) \rightarrow -\pi/2$ as $\xi \rightarrow +\infty$.

5. Wells of $V_{\text{RWA}}(x)$: They all have non-dimensional length π , which corresponds to a length of half the wavelength of the field, that is, $\lambda_0/2 = \pi/k_N^0$. Moreover, the depth of the wells increases as the the transparency of the mirror decreases, that is, as $\xi \rightarrow +\infty$.

6. Maximizers of $f_{\text{RWA}}(x)$: They are denoted by x_{2n} with $n \in \mathbb{Z}^+$. For $\xi \gtrsim 5$ and $n \in \mathbb{Z}^+$ one has to good approximation

$$x_{2n} \simeq n\pi + \frac{1}{\xi}, \quad f_{\text{RWA}}(x_{2n}) \simeq \frac{\xi^2}{2}. \quad (35)$$

7. Minimizers of $f_{\text{RWA}}(x)$: They are denoted by x_{2n+1} with $n \in \mathbb{Z}^+$. For $\xi \gtrsim 5$ and $n \in \mathbb{Z}^+$ one has to good approximation

$$x_{2n+1} \simeq \left(n + \frac{1}{2} \right) \pi + \frac{1}{\xi}, \quad f_{\text{RWA}}(x_{2n+1}) \simeq -\frac{1}{2} \quad (36)$$

8. Zeros of $f_{\text{RWA}}(x)$: They are the maximizers x_n^* and minimizers x_n^{**} of $V_{\text{RWA}}(x)$.

9. Approximation by a Lorentzian: If $\xi \geq 1$ and $x \geq 0$ and $(2m-1)\pi/2 \leq x \leq (2m+1)\pi/2$ for some $m \in \mathbb{Z}^+$, then

$$f_{\text{RWA}}(x) \simeq -\frac{1}{2} + \frac{1}{2\xi^2} \left(\frac{1}{u^2 + \xi^{-4}} \right), \quad (37)$$

with $u = x - (m\pi + 1/\xi)$. One should expect the approximation to be accurate if $1 \gg 3^{-1}(u + \xi^{-1})^2$ and $\xi \gg 1$. Calculating numerically the relative error between $f_{\text{RWA}}(x)$ and the displaced Lorentzian on the right-hand side of (37), we found that the displaced Lorentzian approximates well $f_{\text{RWA}}(x)$ if $\xi \gtrsim 10$ and $-1/\xi < u < 1/\xi$.

The non-dimensional potential $V(x, t)$ has the same periodic structure in x as $V_{\text{RWA}}(x)$. Both its maximizers and minimizers are exactly the same as those of $V_{\text{RWA}}(x)$ and its absolute maximum value is still 0. The only difference is that its absolute minimum value oscillates between 2 times that of $V_{\text{RWA}}(x)$ and 0. This is illustrated in Fig. 2b.

Before proceeding we mention that using (25) one can introduce dimensions so that (27) takes the form

$$M_0 \ddot{q}(t) = \left(\frac{g_0 \omega_0}{\pi c} \right)^2 [1 + \cos(\Omega \tau)] f_{\text{RWA}} [k_N^0 q(t)] , \\ = - \frac{\partial}{\partial x} \left(\frac{g_0 \omega_0}{\pi c} \right)^2 [1 + \cos(\Omega \tau)] V_{\text{RWA}}(x) \Big|_{x=k_N^0 q(t)} . \quad (38)$$

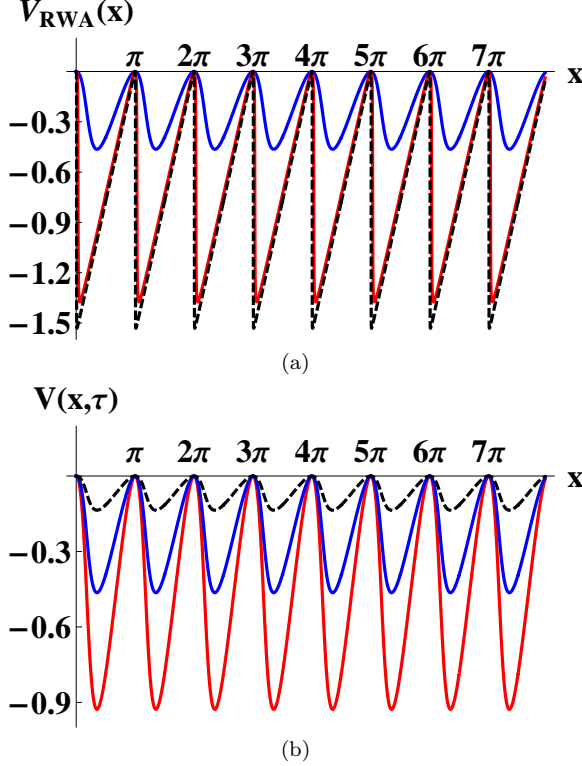


FIG. 2: (Color online) Figure 2a shows $V_{\text{RWA}}(x)$ for $\xi = 1$ (blue-solid line), 10 (red-solid line), and 50 (black-dashed line). Figure 2b shows $V(x, t)$ for $\xi = 1$ and $\Omega \tau = 0$ (red-solid line), $\pi/2$ (blue-solid line), and $3\pi/4$ (black-dashed line).

A. Approximation for $V_{\text{RWA}}(x)$

From Fig. 2a it is clear that $V_{\text{RWA}}(x)$ tends to a *saw tooth wave* as $\xi \rightarrow +\infty$. Hence, it can be approximated by a continuous linear interpolating polynomial for sufficiently large ξ (say, $\xi \gtrsim 50$), that is, $V_{\text{RWA}}(x)$ can be approximated as follows:

$$V_{\text{RWA}}(x) \simeq V_{\text{RWA}}^{\text{approx}}(x) , \quad (39)$$

with

$$V_{\text{RWA}}^{\text{approx}}(x) \equiv \begin{cases} 0 & \text{if } n\pi \leq x \leq n\pi + \frac{1}{\xi} , \\ V_{\text{RWA}}\left(\frac{2}{\xi}\right) & \text{if } n\pi + \frac{1}{\xi} < x \leq n\pi + \frac{2}{\xi} , \\ V_{\text{RWA}}\left(\frac{2}{\xi}\right) + m_+ \left[x - \left(n\pi + \frac{2}{\xi} \right) \right] & \text{if } n\pi + \frac{2}{\xi} \leq x \leq (n+1)\pi . \end{cases} \quad (40)$$

for $n\pi \leq x \leq (n+1)\pi$, $n \in \mathbb{Z}^+$. Here

$$m_+ = - \frac{V_{\text{RWA}}(2/\xi)}{\pi - 2/\xi} . \quad (41)$$

We note that the point $x = (n\pi + 1/\xi)$ corresponds (approximately) to a maximizer x_{2n} of $f_{\text{RWA}}(x)$, see (35).

Figure 3a compares the exact $V_{\text{RWA}}(x)$ with the approximate $V_{\text{RWA}}^{\text{approx}}(x)$ for one of the potential wells and $\xi = 50$. Also, figure 3b illustrates the relative error $|V_{\text{RWA}}(x) - V_{\text{RWA}}^{\text{approx}}(x)|/|V_{\text{RWA}}(x)|$ for $\xi_1 = 50$ (black-dotted line), $\xi_2 = 100$ (blue-dashed line), $\xi_3 = 150$ (red-solid line). From the figures it is clear that the approximation is very good except at thin layers at $x = 4\pi$, $x = (4\pi + 1/\xi)$, and $x = 5\pi$. The reason for this is that $V_{\text{RWA}}^{\text{approx}}(x)$ does not take into account the curvature of the potential. Nevertheless, the region over which $V_{\text{RWA}}^{\text{approx}}(x)$ is a good approximation of $V_{\text{RWA}}(x)$ increases as $\xi \rightarrow +\infty$.

From (30) and (40) it follows that

$$f_{\text{RWA}}(x) \simeq \begin{cases} 0 & \text{if } n\pi < x < \left(n\pi + \frac{2}{\xi} \right) \text{ and} \\ & x \neq \left(n\pi + \frac{1}{\xi} \right) , \\ -m_+ & \text{if } \left(n\pi + \frac{2}{\xi} \right) < x < (n+1)\pi . \end{cases} \quad (42)$$

Hence, for large ξ the function $f_{\text{RWA}}(x)$ is approximately a (non-dimensional) piecewise constant force whose magnitude and direction depends on whether the mirror is to the right or to the left of the minimizer $x_n^{**} \simeq n\pi + 2/\xi$ of the potential $V_{\text{RWA}}(x)$.

IV. DYNAMICS DUE TO RADIATION PRESSURE

Equation (27) is a second order non-linear and non-autonomous differential equation. In the first subsection below we make an approximation that eliminates the time dependence and transforms it into an autonomous differential equation. In the second subsection we discuss the general case.

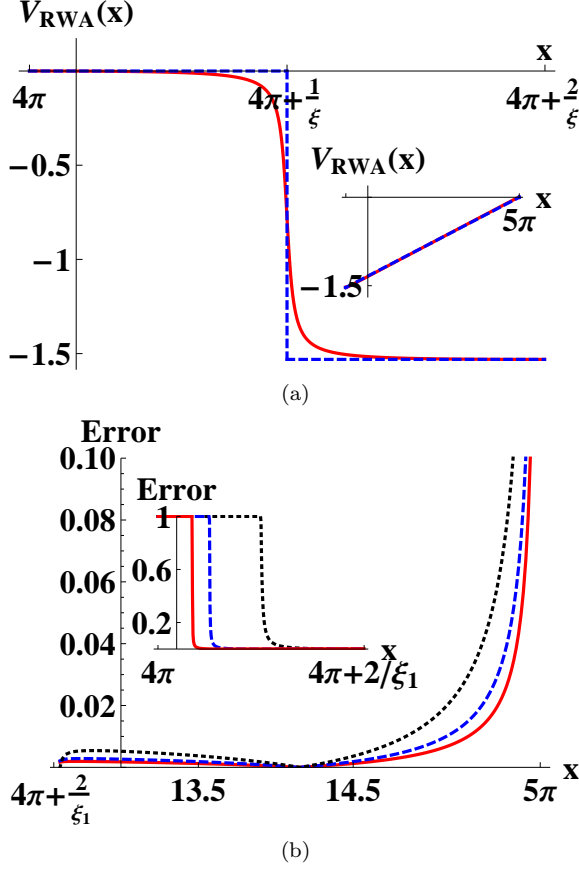


FIG. 3: (Color online) Figure 3a shows a close up of one of the wells of $V_{\text{RWA}}(x)$ (red-solid line) and the approximate $V_{\text{RWA}}^{\text{approx}}(x)$ (blue-dashed line) for $\xi = 50$ and the region $[4\pi, 4\pi + 2\xi^{-1}]$. The inside figure shows the region $[4\pi + 2\xi^{-1}, 5\pi]$. Figure 3b illustrates the relative error $|V_{\text{RWA}}(x) - V_{\text{RWA}}^{\text{approx}}(x)|/|V_{\text{RWA}}(x)|$ for $\xi_1 = 50$ (black-dotted line), $\xi_2 = 100$ (blue-dashed line), and $\xi_3 = 150$ (red-solid line). The inside figure shows a close-up of the interval $[4\pi, 4\pi + 2/\xi_1]$.

A. The limits of low and high field intensity

The limit of low field intensity or RWA regime is defined by the condition

$$\frac{2\pi}{\Omega} \ll P, \quad (43)$$

where P is the (non-dimensional) time scale in which $x(\tau)$ changes appreciably. The name *low field intensity* comes from the fact that $2\pi/\Omega$ is proportional to g_0 , while the name *RWA regime* comes from the fact that the condition in (43) needs to be satisfied in order to be able to perform the RWA.

In the RWA regime the term $\cos(\Omega\tau)$ in (27) oscillates very rapidly and averages to zero. Hence, one can perform the RWA to obtain the approximate equation

$$\frac{d^2x}{d\tau^2}(\tau) = f_{\text{RWA}}[x(\tau)]. \quad (44)$$

The RWA regime appears to be a natural setting for the model under study, since a typical value is $\Omega \geq 10^9$ (see Appendix III). This large value of $\Omega = 2\omega_0/\Delta$ comes from the fact that there are two separate time scales: the characteristic time for the evolution of the field $2\pi/\omega_0$ which is much smaller than the characteristic time for the evolution of the mirror $1/\Delta$.

On the other hand, the limit of high field intensity is defined by the condition

$$\Omega \rightarrow 0. \quad (45)$$

The name *high field intensity* comes from the fact that Ω is inversely proportional to g_0 .

In the limit of high field intensity (27) can be approximated by

$$\frac{d^2x}{d\tau^2}(\tau) = 2f_{\text{RWA}}[x(\tau)]. \quad (46)$$

Although (46) is exactly valid for $\Omega = 0$, it is only valid for $0 \leq \tau \leq \tau_{\text{max}}$ with $|\Omega\tau_{\text{max}}| \ll 1$ if $\Omega > 0$.

In order to treat (44) and (46) simultaneously we define

$$a_0 = \begin{cases} 1 & \text{in low intensity limit,} \\ 2 & \text{in high intensity limit.} \end{cases} \quad (47)$$

Then (44) and (46) can be written as

$$\frac{d^2x}{d\tau^2}(\tau) = a_0 f_{\text{RWA}}[x(\tau)]. \quad (48)$$

We now analyze and solve to good approximation (48).

From (48) one finds that the (non-dimensional) energy $E[x(\tau), x'(\tau)]$ of the movable mirror is conserved and is given by

$$E[x(\tau), x'(\tau)] = \frac{1}{2}[x'(\tau)]^2 + a_0 V_{\text{RWA}}[x(\tau)], \quad (49)$$

Figure 4 shows a contour plot of the energy as a function of x and x' for $\xi = 1$ and $a_0 = 1$ (the RWA regime).

Since the mirror moves under the potential $a_0 V_{\text{RWA}}(x)$ and energy is conserved, it follows that its motion is bounded to one of the wells if and only if $E(x, x') \leq 0$. In this case the movable mirror has a periodic trajectory and acquires its maximum speed v_0 when it is located at one of the minimizers x_n^{**} of the potential $a_0 V_{\text{RWA}}(x)$. Moreover, the requirement that $E(x, x') \leq 0$ is equivalent to the following condition on v_0 :

$$v_0 \leq \sqrt{2a_0 |V_{\text{RWA}}(x_n^{**})|} \leq \sqrt{\pi a_0}. \quad (50)$$

In the last inequality we used (34).

Also, the maximizers $x_n^* = n\pi$ of $a_0 V_{\text{RWA}}(x)$, see (32), are points of unstable equilibrium, since a linear stability analysis of the first order system equivalent to (48) shows that $(x, x') = (n\pi, 0)$ are saddle points (See Theorem 3 in Section 2.10 of [31]).

Recall that a fixed point (or equilibrium point or critical point) of the first order system equivalent to (48) is

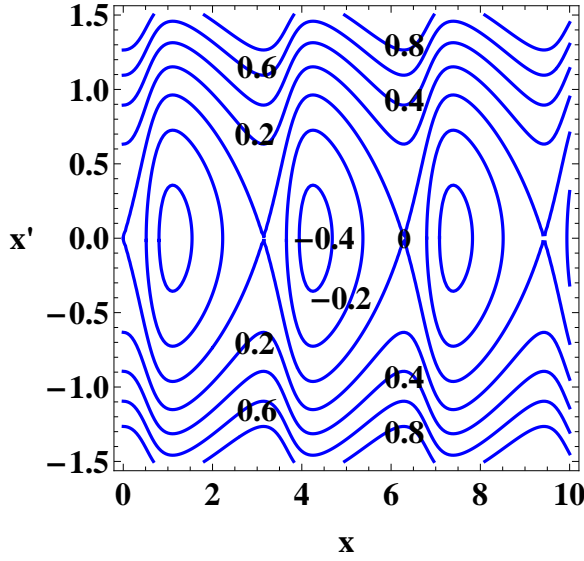


FIG. 4: (Color online) The figure shows a contour plot of the (non-dimensional) energy $E(x, x')$ of the movable mirror as a function of x and x' for $\xi = 1$. The contours $E(x, x') = \pm 0.4, \pm 0.2, 0, 0.6, 0.8$ are shown.

a saddle point if there exist two phase space trajectories that approach the fixed point as $\tau \rightarrow +\infty$ and two phase space trajectories that approach the fixed point as $\tau \rightarrow -\infty$ and if there is a neighborhood V of the fixed point such that all other phase space trajectories which start in the deleted neighborhood associated with V leave V as $\tau \rightarrow \pm\infty$. Here a deleted neighborhood of a fixed point is a neighborhood of the fixed point that does not contain the fixed point.

One can understand the bounded periodic motion of the movable mirror by analyzing the behavior of the mode $V_{k_N^0}[x, q(t)]$ of $A_0(x, t)$ in (24). Assume that the mirror is initially located at a position $q(t) = q_{2n}$ such that ω_0 coincides with one of the cavity resonance frequencies, see (13). Then $V_{k_N^0}[x, q(t)]$ will be very large inside the cavity and small outside of it, see Fig. 5a. As a result, the mirror is pushed to the right. As the mirror moves to the right, ω_0 will become very different from one of the cavity resonance frequencies and $V_{k_N^0}[x, q(t)]$ will decrease inside the cavity. At some point $V_{k_N^0}[x, q(t)]$ will be smaller inside the cavity than outside of it, see Fig. 5b. As a result, the mirror will slow down and eventually start moving to the left. Then the mirror will approach the *resonant position* q_{2n} and, as a result, $V_{k_N^0}[x, q(t)]$ will increase inside the cavity. At some point it will be larger inside the cavity than outside of it, see Fig. 5a. The mirror will then slow down and eventually start moving to the right again. This process repeats itself over and over giving rise to the periodic motion. Therefore, the bounded motion of the mirror is determined by the mirror approaching or withdrawing from a position where the frequency of the field (approximately) coincides with one of the cavity resonance frequencies. Notice that in

the case of bounded motion and $\xi \gtrsim 5$, there is only one position of the mirror, namely $kq_{2n} = x_{2n} \simeq n\pi + 1/\xi$ for some $n \in \mathbb{Z}^+$, such that the frequency ω_0 of the field coincides with one of the cavity resonances.

The unbounded motion of the mirror is understood by referring to the potential $V_{\text{RWA}}(x)$. If the movable mirror has positive energy (see Fig. 4), then it accelerates (decelerates) as it approaches a minimizer (maximizer) of $V_{\text{RWA}}(x)$. In this case radiation pressure is never sufficiently large so as to decelerate the mirror to a complete stop as in the case of the bounded motion.

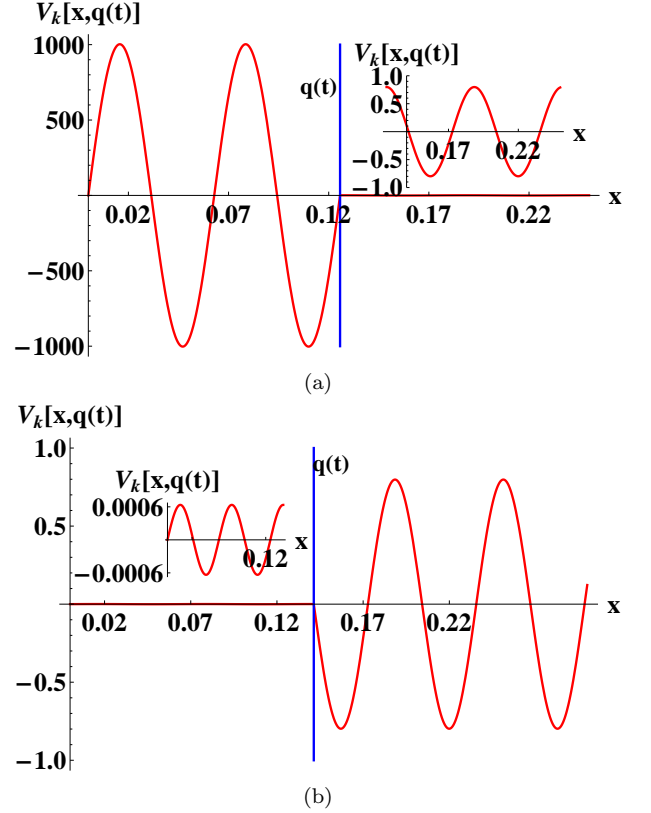


FIG. 5: (Color online) The figures illustrate $V_{k_N^0}[x, q(t)]$ as a function of x when the movable mirror is located at the position $q(t)$ with $\chi_0 = 1$ m, $k_N^0 = 100$ m $^{-1}$, $n = 4$, and $\xi = 4\pi\chi_0 k_N^0 = 4\pi \times 100$. In all figures the vertical blue line shows the position of the movable mirror. In Fig. 5a $k_N^0 q(t) = n\pi + 1/\xi$ and ω_0 coincides with one of the cavity resonance frequencies. The inside figure shows $V_{k_N^0}[x, q(t)]$ outside of the cavity. In Fig. 5b $k_N^0 q(t) = (n + 1/2)\pi$ is such that ω_0 is very different from all cavity resonance frequencies. The inside figure shows $V_{k_N^0}[x, q(t)]$ inside the cavity.

Now assume that $\xi \gg 1$ (say, $\xi \gtrsim 50$), that is, the mirror has small transparency. In this case one can use the approximation in (40) for $V_{\text{RWA}}(x)$ to solve analytically equation (48). We shall only consider the case in which $E(x, x') < 0$. Notice that one cannot describe accurately the bounded motion of the mirror in a small

band around $E(x, x') = 0$, since the mirror cannot approach $x = n\pi$ with the approximation in (40).

Assuming that the moving mirror is in the n -th well and pasting the solutions one gets that

$$x_{\text{RWA}}(\tau) = \begin{cases} \left(n\pi + \frac{2}{\xi}\right) + v_0(\tau - \tau_{2k}) - a_0 \frac{m_+}{2}(\tau - \tau_{2k})^2 & \text{if } \tau_{2k} \leq \tau \leq \tau_{2k+1}, \\ \left(n\pi + \frac{2}{\xi}\right) - v_0(\tau - \tau_{2k+1}) & \text{if } \tau_{2k+1} \leq \tau \leq \tau'_{2k+1}, \\ \left(n\pi + \frac{1}{\xi}\right) + v_0(\tau - \tau'_{2k+1}) & \text{if } \tau'_{2k+1} \leq \tau \leq \tau_{2(k+1)}. \end{cases} \quad (51)$$

Here $k \in \mathbb{Z}$ and τ_0 is an instant such that $x(\tau_0) = n\pi + 2/\xi$ and $v_0 = (dx/d\tau)(\tau_0) > 0$ is the maximum (non-dimensional) speed of the mirror. For $k \in \mathbb{Z}$ one has

$$\begin{aligned} \tau_{2k+1} - \tau_{2k} &= \frac{2v_0}{a_0 m_+}, \\ \tau_{2(k+1)} - \tau'_{2k+1} &= \tau'_{2k+1} - \tau_{2k+1} = \frac{1}{\xi v_0}. \end{aligned} \quad (52)$$

Observe that $x(\tau_{2k}) = n\pi + 2/\xi$ and $v_0 = (dx/d\tau)(\tau_{2k})$ for all $k \in \mathbb{Z}$.

From (51) and (52) one finds that the bounded motion has period P given by

$$P = \frac{2v_0}{a_0 m_+} + \frac{2}{\xi v_0}. \quad (53)$$

The absolute minimum value P_{\min} of P occurs for $v_0 = \sqrt{a_0 m_+/\xi} \simeq \sqrt{a_0/(2\xi)}$ and is given by

$$P_{\min} = \frac{4}{\sqrt{a_0 m_+ \xi}} \simeq 4\sqrt{\frac{2}{a_0 \xi}}. \quad (54)$$

Here we used (41) to conclude that $m_+ \simeq 1/2$ for $\xi \gg 1$.

Figure 6 shows $x(\tau)$ (red-solid line) obtained by solving numerically (44) for $\xi = 50$ and the initial conditions $x(0) = 4\pi + 1/\xi$ and $x'(0) = 0$. These initial conditions are such that the movable mirror starts from rest at a position where ω_0 coincides with one of the cavity resonance frequencies. Also, $\mathcal{E} \equiv E(4\pi + 1/\xi, 0)$ is the energy of the movable mirror. The figure also shows the approximate solution $x_{\text{RWA}}(\tau)$ (blue-dashed line) given in (51) and corresponding to the same energy \mathcal{E} . Notice that one has to adjust the initial velocity of the movable mirror in order to apply (51). According to the approximation in (40) the corresponding initial conditions for $x_{\text{RWA}}(\tau)$ are $x(0) = 4\pi + 1/\xi$ and $x'(0) = x'_0(0)$ with

$$x'_0(0) = \sqrt{2 \left[\mathcal{E} - a_0 V_{\text{RWA}} \left(\frac{2}{\xi} \right) \right]}. \quad (55)$$

Observe that the agreement between $x(\tau)$ and $x_{\text{RWA}}(\tau)$ is quite good.

To end this subsection we establish the regime of validity of the model, that is, we determine when (5) are valid and we rewrite conditions (43) and (45) for the low and high intensity limits. In the following we drop the assumption that $\xi \gg 1$ and we do not restrict the motion to be bounded.

From (49) we know that energy is conserved, that is,

$$E[x(\tau), x'(\tau)] = E_0 \quad (\tau \in \mathbb{R}). \quad (56)$$

From (49) and (56) one can solve for $x'(\tau)$ and then use the bounds in (34) to conclude that

$$|x'(\tau)| \leq v_{\max} \equiv \sqrt{2E_0 + a_0 \pi}. \quad (57)$$

From the definition of $x(\tau)$ in (25) one can relate $x'(\tau)$ and $x''(\tau)$ with $\dot{q}(t)$ and $\ddot{q}(t)$ as follows:

$$\frac{\dot{q}(t)}{c} = \frac{2}{\Omega} x'(\tau), \quad \frac{\ddot{q}(t)}{c\omega_0} = \frac{4}{\Omega^2} x''(\tau). \quad (58)$$

Recall that $\tau = \Delta t$.

Combining (57) with (58) one obtains a sufficient condition for the first part of (5) to be valid:

$$2\sqrt{2E_0 + a_0 \pi} \ll \Omega \Rightarrow \left| \frac{\dot{q}(t)}{c} \right| \ll 1 \quad (t \in \mathbb{R}). \quad (59)$$

To get an idea of the order of magnitude of the quantities involved in (59) we take from Appendix III the typical value $\Omega \geq 10^9$. Since $E_0 \leq 0$ for bounded motion and $a_0 \leq 2$, one has $2\sqrt{2E_0 + a_0 \pi} \leq 2\sqrt{2\pi} \ll 10^9 \leq \Omega$ for bounded motion. From (59) it follows that $|\dot{q}(t)/c| \ll 1$ for all $t \in \mathbb{R}$ if only bounded motion is considered.

We now consider the second part of (5). From (44)-(47) one finds that

$$|x''(\tau)| \leq a_0 f_{\text{RWA}}(x_{2n}) \quad (\tau \in \mathbb{R}), \quad (60)$$

where x_{2n} is a maximizer of $f_{\text{RWA}}(x)$, see (35). Combining (58) with (60) one obtains a sufficient condition for the second part of (5) to be valid:

$$4a_0 f_{\text{RWA}}(x_{2n}) \ll \Omega^2 \Rightarrow \left| \frac{\ddot{q}(t)}{c\omega_0} \right| \ll 1 \quad (t \in \mathbb{R}). \quad (61)$$

To get an idea of the order of magnitude of the quantities involved in (61) we take from Appendix III the typical values $\xi = 6.4$ (which corresponds to a reflectivity of the movable mirror of 0.91) and $\Omega \geq 10^9$. Since $a_0 \leq 2$ and $f_{\text{RWA}}(x_{2n}) \simeq \xi^2/2 = 20.48$ (see (35)), it follows that $4a_0 f_{\text{RWA}}(x_{2n}) \lesssim 163.84 \ll 10^{18} \leq \Omega^2$. From (61) one then obtains that $|\ddot{q}(t)/(c\omega_0)| \ll 1$ for all $t \in \mathbb{R}$. Observe that this condition is valid for both bounded and unbounded motion. It follows that the model presented in Sec.II is an accurate description of the physical system under study.

If one considers only bounded motion (that is, $E_0 \leq 0$) and that the transparency of the movable mirror is very

small (that is, $\xi \gg 1$), then it follows from (59) and (61) that

$$4\xi^2 \ll \Omega^2 \Rightarrow \left| \frac{\ddot{q}(t)}{c\omega_0} \right|, \left| \frac{\dot{q}(t)}{c} \right| \ll 1 \quad (t \in \mathbb{R}). \quad (62)$$

Here we have used $a_0 \leq 2$ and $f_{\text{RWA}}(x_{2n}) \simeq \xi^2/2$, see (35). To illustrate the order of magnitude of the quantities in (62) we take from Appendix III the values $\xi = 50$ (which corresponds to a reflectivity of the movable mirror of 0.9984) and $\Omega \geq 10^9$. It follows that $4\xi^2 = 10^4 \ll 10^{18} \leq \Omega^2$. It follows from (62) that the conditions in (5) are satisfied.

Consider the high field limit condition in (45). The latter requires $\Omega \ll 1$, while the sufficient conditions in (59) and (61) essentially need $\Omega \gg 1$ (see also (62) for the case $\xi \gg 1$ and $E_0 \leq 0$). Therefore, the high field limit appears to be incompatible with the model presented in the first section, that is, the field does not see the movable mirror as fixed in the high field limit. Notice that this result is reasonable, since a very strong field could subject the mirror to large accelerations (for $\xi \gtrsim 5$ the condition $|\ddot{q}(t)/(c\omega_0)| = |4x''(\tau)/\Omega^2| \ll 1$ can break down because $x''(\tau)$ can take the value $f_{\text{RWA}}(x_{2n}) \simeq \xi^2/2$ which is large).

Finally, we turn to the case of the low intensity limit (or, RWA regime) in the case of bounded motion, that is, $E_0 \leq 0$. The condition for this regime is still given by (43) but with P the period of the bounded motion. In the case $\xi \gg 1$ (that is, the transparency of the movable mirror is very small) one can use (54) to obtain a general sufficient condition for the RWA to be valid:

$$\Omega \gg \frac{\pi}{2} \sqrt{m_+ \xi} \simeq \frac{\pi}{2} \sqrt{\frac{\xi}{2}}. \quad (63)$$

Comparing (63) with (62) one realizes that the low intensity limit (or RWA regime) is the natural setting for the consideration of the model established in the first section in the case where the transparency of the movable mirror is small (that is, $\xi \gg 1$).

B. The intermediate case

In this subsection we consider equation (27) without making any assumptions on Ω . As expected, the dynamics are much more complex in this case. If the movable mirror is initially confined to one of the wells of $V_{\text{RWA}}(x)$, at future times it may jump out of the well and then be confined for some time in another well. Figure 7a illustrates this type of behavior for $\xi = 50$, $\Omega = 1000, 1500$, and 2000 , and the initial conditions $x(0) = 4\pi + 1/\xi$, $x'(0) = 0$ so that initially ω_0 (approximately) coincides with one of the cavity resonance frequencies. Also, oscillations in one well similar to those obtained with the RWA in the previous subsection are possible for large enough Ω . Figure 7b illustrates this type of behavior for $\Omega = 5000$ (blue-dashed line) and $\Omega = 10000$ (red-solid line) and compares it with the solution in the RWA

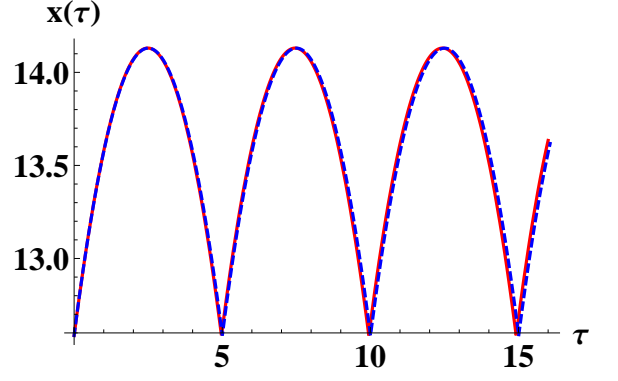


FIG. 6: (Color online) The figure illustrates the solution $x(\tau)$ (red-solid line) of (44) computed numerically for $\xi = 50$ and the initial conditions $x(0) = 4\pi + 1/\xi$, $x'(0) = 0$. It also shows the approximate solution $x_{\text{RWA}}(\tau)$ (blue-dashed line) in (51) with $a_0 = 1$ corresponding to the same energy $\mathcal{E} = E(4\pi + 1/\xi, 0)$.

The corresponding initial conditions for $x_{\text{RWA}}(\tau)$ are $x(0) = 4\pi + 1/\xi$ and $x'(0) = x'_0(0)$ with $x'_0(0)$ in (55).

(black-dot-dashed line) calculated numerically from (44). Notice how $x(\tau)$ tends to the solution in the RWA for increasing Ω . Figure 7b uses the same value of ξ and the same initial conditions as Fig. 7a.

We now discuss the regime of validity of the model presented in Sec.II, that is, we obtain sufficient conditions for (5) to be valid.

If $|x'(\tau)| \leq v_{\text{max}}$ for all τ , it follows from (58) that

$$2v_{\text{max}} \ll \Omega \Rightarrow \left| \frac{\dot{q}(t)}{c} \right| \ll 1 \quad (t \in \mathbb{R}), \quad (64)$$

The problem here is that there is no direct way to bound the velocity as in the case of the RWA regime because energy is no longer conserved. We now illustrate (64) using the parameters of Fig. 6, that is, $\xi = 50$ and $\Omega \geq 1000$. All the numerical solutions in Fig. 6 have $|x'(\tau)| \leq 2.3$ for the τ interval shown, so that $2v_{\text{max}} \leq 4.6 \ll 1000 \leq \Omega$. Hence, it follows from (64) that the first condition in (5) is satisfied for the parameters of Fig. 6.

From (27) one has

$$|x''(\tau)| \leq 2f_{\text{RWA}}(x_{2n}) \quad (t \in \mathbb{R}), \quad (65)$$

with x_{2n} a maximizer of $f_{\text{RWA}}(x)$. Using (58) it follows that

$$8f_{\text{RWA}}(x_{2n}) \ll \Omega^2 \Rightarrow \left| \frac{\ddot{q}(t)}{c\omega_0} \right| \ll 1 \quad (t \in \mathbb{R}). \quad (66)$$

We illustrate (66) using the parameters of Fig. 6. Since $\xi = 50$ and $\Omega \geq 1000$, one has from (35) that $8f_{\text{RWA}}(x_{2n}) \simeq 10^4 \ll 10^6 \leq \Omega^2$. From (66) it follows that the second condition in (5) is satisfied for the parameters of Fig. 6.

It is important to note that $8f_{\text{RWA}}(x_{2n}) \ll \Omega^2$ implies that $\Omega \gg 1$. For example, if the reflectivity of the

mirror is 0.91 for the mode of the field, then $\xi = 6.4$ (see Appendix III) and $x_{2n} \simeq n\pi + 1/\xi$ to good approximation (see (35)). From (35) it then follows that $8f_{\text{RWA}}(x_{2n}) \simeq 163.84$. Hence, $8f_{\text{RWA}}(x_{2n}) \ll \Omega^2$ would require $160.84 \ll \Omega^2$ (say $10^4 \leq \Omega^2$). This observation is more evident in the case where the transparency of the mirror is small, since $8f_{\text{RWA}}(x_{2n}) \ll \Omega^2$ takes the form $4\xi^2 \ll \Omega^2$ if $\xi \gg 1$. Here we used (35).

To end this subsection we note that (40) can be used to solve (27) approximately if $\xi \gg 1$. We do not pursue this direction here.

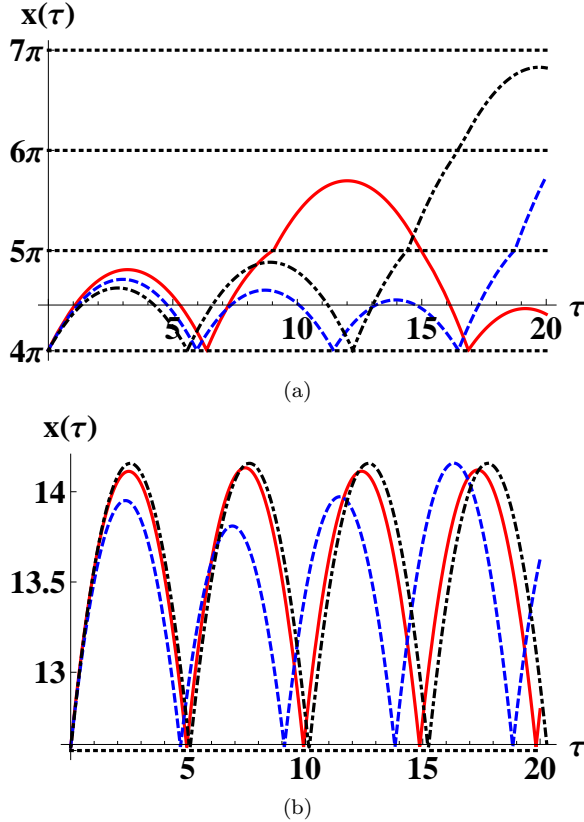


FIG. 7: (Color online) Figure 7a illustrates $x(\tau)$ computed numerically from (27) with $\Omega = 2000$ (black-dot-dashed line), 1500 (blue-dashed line), 1000 (red-solid line). The horizontal black-dotted lines at 4π , 5π , 6π , and 7π indicate the beginning and the ends of the potential wells of $V_{\text{RWA}}(x)$. Figure 7b illustrates $x(\tau)$ computed numerically from (27) for $\Omega = 10000$ (red-solid line) and $\Omega = 5000$ (blue-dashed line). It also illustrates the solution in the RWA (black-dot-dashed line) calculated numerically from (44) and the constant function 4π (black-dotted line) indicating the beginning of a well of $V_{\text{RWA}}(x)$. Both figures have $\xi = 50$ and the initial conditions $x(0) = 4\pi + 1/\xi$ and $x'(0) = 0$.

V. INTRODUCTION OF FRICTION

In this section we assume that the movable mirror is subject to friction linear in the velocity. For example, one could think that the mirror is attached to a set of wheels that subjects it to friction and allows it to move due to the radiation pressure exerted by the field. In this case the equation of motion for the mirror is given by

$$\frac{d^2x}{d\tau^2}(\tau) + \Gamma \frac{dx}{d\tau}(\tau) = [1 + \cos(\Omega\tau)] f_{\text{RWA}}[x(\tau)] . \quad (67)$$

We note that (67) is obtained by adding on the right of (8) the friction force $-\gamma\dot{q}(t)$ and then using (25) to express the equation in terms of non-dimensional quantities. Here γ has units of Ns/m^3 and $\Gamma = \gamma/(\Delta M_0)$ is a non-dimensional quantity.

As before we shall consider the limit of low and high field intensity and the intermediate case separately.

A. The limit of low and high field intensity

The limit of low field intensity is still defined by condition (43) and it allows one to perform the RWA in (67). On the other hand, the limit of high field intensity is still given by (45). Hence, (67) can be approximated by

$$\frac{d^2x}{d\tau^2}(\tau) + \Gamma \frac{dx}{d\tau}(\tau) = a_0 f_{\text{RWA}}[x(\tau)] , \quad (68)$$

with a_0 given in (47).

We now perform a linear stability analysis of (68). The aforementioned equation can be written as a first order non-linear system as follows:

$$\begin{aligned} \frac{d}{d\tau} \begin{pmatrix} x(\tau) \\ y(\tau) \end{pmatrix} &= \mathbf{f}[x(\tau), y(\tau)] , \\ &\equiv \begin{pmatrix} y(\tau) \\ -\Gamma y(\tau) + a_0 f_{\text{RWA}}[x(\tau)] \end{pmatrix} , \end{aligned} \quad (69)$$

with $y(\tau) = x'(\tau)$. Using (30) it follows that the fixed points of (69) are determined by the maximizers and minimizers of $V_{\text{RWA}}(x)$. Explicitly, the fixed points of (69) are given by $(x_n^*, y_n^*) = (n\pi, 0)$ and $(x_n^{**}, y_n^{**}) \simeq (n\pi + 2/\xi, 0)$ with $n \in \mathbb{Z}^+$, see (32) and (33).

The linearization of (69) at the fixed points reveals that $(x_n^*, y_n^*) = (n\pi, 0)$ are saddle points (see Theorem 3 in Section 2.10 of [31]) and that $(x_n^{**}, y_n^{**}) \simeq (n\pi + 2/\xi, 0)$ are attractors (see Theorem 4 in Section 2.10 of [31]).

Recall that a fixed point is an attractor if there is a neighborhood V of the fixed point such that any phase space trajectory $(x(\tau), y(\tau))$ that starts in V tends to the fixed point as $\tau \rightarrow +\infty$.

In particular, the attractors are stable spirals if

$$\frac{\Gamma}{2} < \sqrt{a_0 |f'_{\text{RWA}}(x_n^{**})|} \simeq \sqrt{a_0 \xi} . \quad (70)$$

On the other hand, the attractors are stable nodes if

$$\frac{\Gamma}{2} \geq \sqrt{a_0 |f'_{\text{RWA}}(x_n^{**})|} \simeq \sqrt{a_0 \xi} . \quad (71)$$

(See Theorem 4 of Section 2.10 of [31]). We note that in (70) and (71) the value on the extreme right is obtained by neglecting terms of order $1/\xi^2$ and smaller with respect to 1.

Recall that a fixed point is called a stable spiral or focus if there is a deleted neighborhood V of the fixed point such that every phase space trajectory $(x(\tau), y(\tau))$ in V spirals toward the fixed point as $\tau \rightarrow +\infty$. On the other hand, a fixed point is called a stable node if there is deleted neighborhood V of the fixed point such that every phase space trajectory $(x(\tau), y(\tau))$ in V approaches the fixed point along a well-defined tangent line as $\tau \rightarrow +\infty$.

Figure 8 illustrates these different types of behaviors for $\xi = 10$ and $a_0 = 1$ (that is, in the RWA regime). Notice that the movable mirror exhibits a behavior similar to an under-damped harmonic oscillator in the case of the stable spiral and to an over-damped harmonic oscillator in the case of a stable node.

Figure 8a also illustrates the stable and unstable manifolds of a saddle point calculated using the linearization of (69). They are given by

$$x' = \lambda_{\pm}(x - n\pi) , \quad (72)$$

with $n \in \mathbb{Z}^+$ and λ_{\pm} the eigenvalues of the coefficient matrix of the linearized system at the saddle point

$$\lambda_{\pm} = -\frac{\Gamma}{2} \pm \sqrt{\left(\frac{\Gamma}{2}\right)^2 + a_0 \xi} . \quad (73)$$

The stable (unstable) manifold corresponds to the minus (plus) sign.

Recall that the stable manifold of a saddle point is the set of initial conditions such that $(x(\tau), y(\tau))$ tends to the saddle point as $\tau \rightarrow +\infty$, while the unstable manifold of a saddle point is the set of initial conditions such that $(x(\tau), y(\tau))$ tends to the saddle point as $\tau \rightarrow -\infty$.

Since $\nabla \cdot \mathbf{f}(x, y) = -\Gamma < 0$ for all $(x, y) \in \mathbb{R}^+ \times \mathbb{R}$ with $\mathbf{f}(x, y)$ in (69), it follows from Bendixon's criterion (see Theorem 1 in Section 3.9 of [31]) that there are no closed orbits and no cycle-graphs in phase space.

Recall that a cycle-graph is also called a compound separatrix cycle and that it is a closed curve in phase space that consists of $N \geq 1$ vertices and at least N edges. The vertices are fixed points and the edges are trajectories that tend to vertices as $\tau \rightarrow \pm\infty$. The whole curve is coherently oriented by increasing time. For a precise statement see Definition 1 in Section 3.7 of [31].

The non-existence of closed orbits and cycle-graphs in phase space could have also been anticipated by noting that the energy of the mirror defined in (49) is always decreasing:

$$E[x(\tau), x'(\tau)] = E[x(0), x'(0)] - \Gamma \int_0^\tau d\tau' [x'(\tau')]^2 .$$

For $\tau \gg 1$ the movable mirror always tends to the position x_n^{**} of a minimizer of $V_{\text{RWA}}(x)$. The only exceptions are the trajectories associated with the stable manifolds of the saddle points in which case the movable mirror tends to a maximizer x_n^* of $V_{\text{RWA}}(x)$. The behavior stated in the previous lines is a consequence of the Poincaré-Bendixon theory in \mathbb{R}^2 (see Section 3.7 of [31]) and the facts that there are no closed orbits and no cycle-graphs in phase space and that the energy of the mirror is always decreasing (so that trajectories in phase space are bounded for $\tau \geq 0$).

Taking $\xi \gtrsim 10$ and using (13), (15), and (35) one finds that the frequency ω_0 of the field approximately coincides with one of the cavity resonance frequencies only if the non-dimensional position $x = k_N^0 q$ of the movable mirror satisfies $|x - x_{2n}| \leq 1/\xi^2$ with $x_{2n} = k_N^0 q_{2n} \simeq n\pi + 1/\xi$. For $\xi \gtrsim 10$ one has $|x - x_{2n}| \simeq 1/\xi \gg 1/\xi^2$ if $x = x_n^* = n\pi$ or $x = x_n^{**} \simeq n\pi + 1/\xi$, see (32) and (33). Therefore, the movable mirror ends up in a position that is very different from one in which ω_0 coincides with one of the cavity resonance frequencies if $\xi \gtrsim 10$.

We now solve analytically (68) to good approximation in the case $\xi \gg 1$ and $E[x(0), x'(0)] < 0$. Using the approximations given in (40) and (42) it follows that the solution $x_{\text{RWA}}(\tau)$ of the aforementioned equation is

$$x_{\text{RWA}}(\tau) = c_2(\tau_0)e^{-\Gamma(\tau-\tau_0)} - a_0 \frac{m_+}{\Gamma}(\tau - \tau_0) + c_1(\tau_0) + a_0 \frac{m_+}{\Gamma^2} \left[1 - e^{-\Gamma(\tau-\tau_0)} \right] , \quad (75)$$

with

$$\begin{aligned} c_1(\tau_0) &= x_{\text{RWA}}(\tau_0) + \frac{1}{\Gamma} x'_{\text{RWA}}(\tau_0) , \\ c_2(\tau_0) &= -\frac{1}{\Gamma} x'_{\text{RWA}}(\tau_0) , \end{aligned} \quad (76)$$

if $(n\pi + 2/\xi) \leq x_{\text{RWA}}(\tau) \leq (n+1)\pi$ for $\tau_0 \leq \tau \leq \tau_1$ and some $n \in \mathbb{Z}^+$. Also,

$$x_{\text{RWA}}(\tau) = x_{\text{RWA}}(\tau_1) + \frac{x'_{\text{RWA}}(\tau_1)}{\Gamma} \left[1 - e^{-\Gamma(\tau-\tau_1)} \right] , \quad (77)$$

if $(n\pi + 1/\xi) \leq x_{\text{RWA}}(\tau) \leq (n\pi + 2/\xi)$ for $\tau_1 \leq \tau \leq \tau_2$. In order to get the complete trajectory, the solutions in (75) and (77) have to be pasted together in order to guarantee the continuity of $x_{\text{RWA}}(\tau)$ and $x'_{\text{RWA}}(\tau)$. Moreover, it has to be taken into account that $x_{\text{RWA}}(\tau)$ bounces elastically from a potential wall if it reaches $(n\pi + 1/\xi)$ (see the approximation in (40)). We omit the details.

Figure 9 compares the approximate $x_{\text{RWA}}(\tau)$ with $x(\tau)$ computed numerically from (68) with $a_0 = 1$ (the RWA regime) for $\xi = 50$ and two values of Γ . The initial conditions are $x(0) = (4\pi + 1/\xi)$ and $x'(0) = 0$, so that the movable mirror starts from rest at a position where ω_0 coincides with one of the cavity resonance frequencies. As in the previous section, in order to use (75) and (77) one has to adjust the initial velocity $x'(0)$ to be

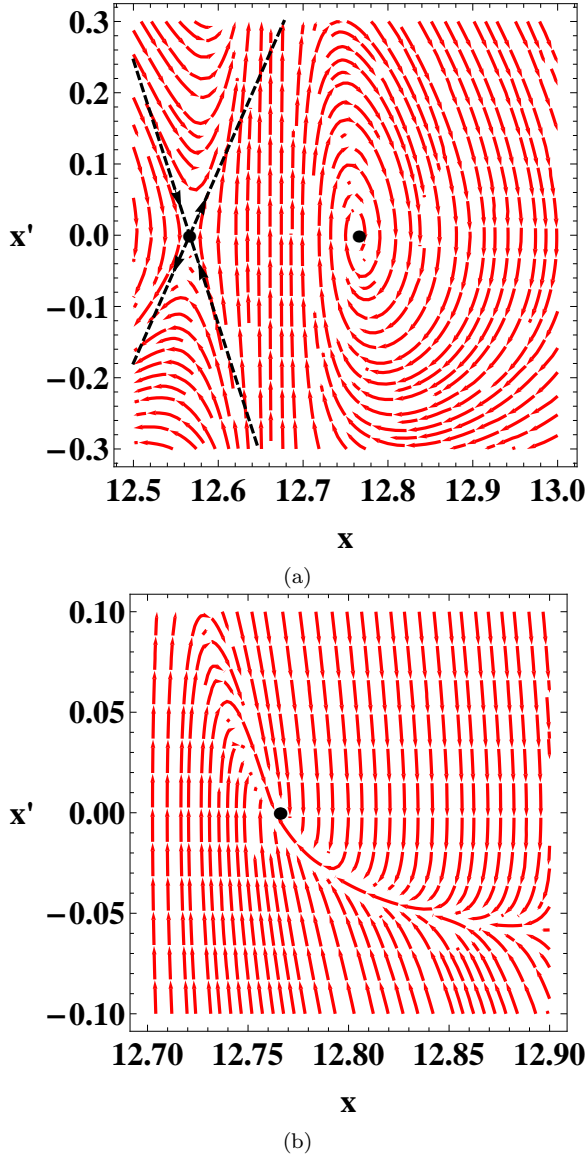


FIG. 8: (Color online) Figure 8a illustrates the phase portrait of the movable mirror in the case $\xi = 10$, $\Gamma = 1$, and $a_0 = 1$ (the RWA regime). The black dot on the left indicates the saddle point $(x_n^*, y_n^*) = (4\pi, 0)$, while the black dot on the right indicates the stable spiral $(x_n^{**}, y_n^{**}) \simeq (4\pi + 2/\xi, 0)$. Also, the black-dashed line with negative (positive) slope indicates the stable (unstable) manifold of the saddle point. Figure 8b illustrates the phase portrait of the movable mirror in the case $\xi = 10$, $\Gamma = 7$, and $a_0 = 1$. The black dot indicates the stable node $(x_n^{**}, y_n^{**}) \simeq (4\pi + 2/\xi, 0)$.

$x'_0(0)$ in (55) with $\mathcal{E} = E(4\pi + 1/\xi, 0)$ the initial energy. Notice that the agreement between the numerical solution and $x_{\text{RWA}}(\tau)$ is quite good for not very large times in Fig. 9a which corresponds to the case where $\Gamma = 1$ and $(x_n^{**}, y_n^{**}) \simeq (4\pi + 2/\xi, 0)$ is a stable spiral. The agreement is not so good in Fig. 9b which corresponds to the case where $\Gamma = 16$ and $(x_n^{**}, y_n^{**}) \simeq (4\pi + 2/\xi, 0)$

is a stable node. The differences between the analytical and the numerical solutions are due to two facts. First, the approximation in (40) does not take into account the curvature of the potential $V_{\text{RWA}}(x)$. Second, for large enough times the movable mirror spends more time near the minimizer x_n^{**} of $V_{\text{RWA}}(x)$ where the curvature is important. Nevertheless, $x_{\text{RWA}}(\tau)$ allows one to understand the behavior of the mirror. From (75) it follows that the movable mirror approximately behaves like a particle in free fall subject to friction (linear in the velocity) when it is in the region between the minimizer $x_n^{**} \simeq (n\pi + 2/\xi)$ and the maximizer $x_{n+1}^* = (n+1)\pi$ of $V_{\text{RWA}}(x)$. On the other hand, from (77) we see that it behaves approximately like a particle subject only to friction in the region between the maximizer $x_{2n} \simeq (n\pi + 1/\xi)$ of $f_{\text{RWA}}(x)$ and x_n^{**} . Moreover, the mirror bounces elastically from an impenetrable potential wall if it reaches x_{2n} , which corresponds to the maximizer of $f_{\text{RWA}}(x)$ (see (35) and (40)).

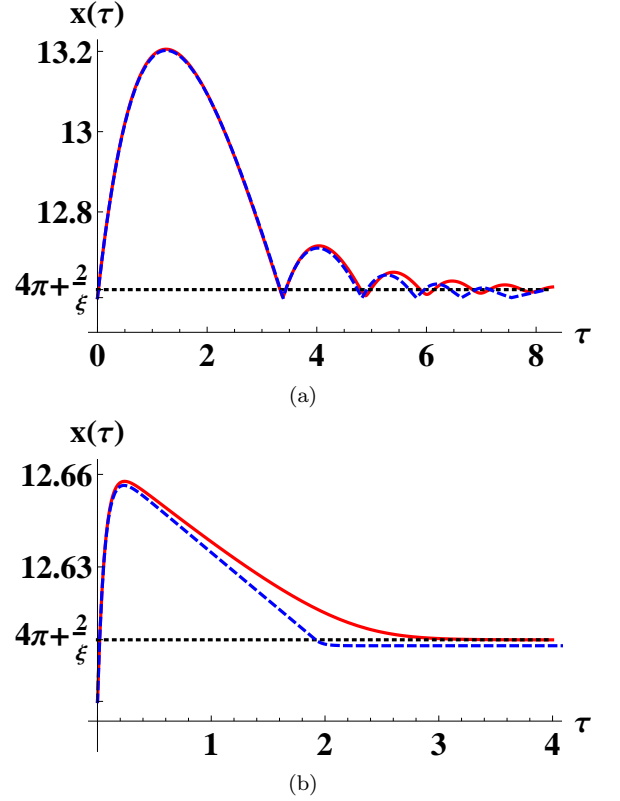


FIG. 9: (Color online) The figures compare the numerical solution (red-solid line) of (68) and the approximate $x_{\text{RWA}}(\tau)$ in (75) and (77) (blue-dashed line) for $a_0 = 1$ (the RWA regime), $\xi = 50$, and the initial conditions $x(0) = (4\pi + 1/\xi)$ and $x'(0) = 0$. Fig. 9a has $\Gamma = 1$, while Fig. 9b has $\Gamma = 16$.

To end this subsection we discuss the regime of validity of the model, that is, we give sufficient conditions for (5) to be valid. Moreover, we use the approximate $x_{\text{RWA}}(\tau)$ to determine the regime of validity of the RWA. In the

following the discussion is general and we do not assume that $\xi \gg 1$ or that $E[x(0), x'(0)] < 0$.

From (49) and (74) it follows that (57) still holds with $E_0 = E[x(0), x'(0)]$ and $\tau \geq 0$. Hence, (59) is still valid with $E_0 = E[x(0), x'(0)]$ and $\tau \geq 0$.

Using (57) with $E_0 = E[x(0), x'(0)]$ and $t \geq 0$ in combination with (58) and (68) it follows that

$$\left| \frac{\ddot{q}(t)}{c\omega_0} \right| \leq \frac{a_0 f_{\text{RWA}}(x_{2n}) + \Gamma \sqrt{2E_0 + a_0 \pi}}{(\Omega/2)^2} \quad (t \geq 0). \quad (78)$$

Here we have used that v_{max} is given in (57) and that x_{2n} is a maximizer of $f_{\text{RWA}}(x)$, see (35). Hence,

$$\begin{aligned} 4a_0 f_{\text{RWA}}(x_{2n}) + 4\Gamma \sqrt{2E_0 + a_0 \pi} &\ll \Omega^2 \\ \Rightarrow \left| \frac{\ddot{q}(t)}{c\omega_0} \right| &\ll 1 \quad (t \geq 0). \end{aligned} \quad (79)$$

Notice that (79) is similar to (61), since it only adds the term $4\Gamma \sqrt{2E_0 + a_0 \pi}$.

As in the case of dynamics due only to radiation pressure, conditions (59) and (79) essentially say that the model applies if Ω is sufficiently large. Using the values $\Gamma/\Omega \sim 10^{-14}$ and $\Omega \sim 10^9$ from Appendix III, it follows that the conditions for the validity of the model presented in Sec. II with the addition of friction (linear in the velocity) basically reduce to those of the case where there is no friction discussed in the previous section if E_0 is not too large.

If $\xi \gg 1$ (that is, the transparency of the movable mirror is very small) and $E_0 \leq 0$ (that is, the movable mirror is initially bounded to one of the potential wells), then conditions (59) and (79) reduce to the following:

$$\begin{aligned} 4\Gamma \sqrt{a_0 \pi} + 2a_0 \xi^2 &\ll \Omega^2 \\ \Rightarrow \left| \frac{\dot{q}(t)}{c} \right|, \left| \frac{\ddot{q}(t)}{c\omega_0} \right| &\ll 1 \quad (t \geq 0). \end{aligned} \quad (80)$$

Here we used (35) to evaluate $f_{\text{RWA}}(x_{2n})$.

Finally we turn to the case of the low and high intensity limits. We first discuss the high intensity limit. Comparing (59) and (79) with (45) it appears that the high intensity limit can be incompatible with the model of Sec. II at the beginning of the motion of the mirror (recall that the mirror ultimately tends to a maximizer or minimizer of $V_{\text{RWA}}(x)$), that is, the field does not *see* the mirror as fixed during the whole evolution in the high intensity limit. This is made more explicit if the transparency of the movable mirror is very small and $E_0 \leq 0$, since one has to compare (45) and (80). Notice that this result is reasonable because a very strong field could subject the mirror to large accelerations before it is approximately found at a minimizer or maximizer of $V_{\text{RWA}}(x)$.

Let us consider the case of the low intensity limit (or RWA regime). We assume that $\xi \gg 1$ (that is, the transparency of the movable mirror is very small) and $E_0 < 0$

(that is, the movable mirror starts in one of the potential wells at time $t = 0$). Since the effect of friction is to slow down the movable mirror to an eventual stop, it follows that the time in which $x(\tau)$ changes appreciably can be estimated by the time in which $x(\tau)$ changes appreciably without friction. Hence, one can take (63) to be a sufficient condition for the RWA to be valid. Again, comparing (63) and (80) it follows that the low intensity limit (or RWA regime) is a natural setting for the model presented in the first section.

B. The intermediate case

In this subsection we go back to (67). As before, the dynamics of the mirror are much more complex in this case. The numerical results show that depending on the values of Ω , Γ , and ξ , the mirror can simply tend to a minimizer of $V_{\text{RWA}}(x)$ in a similar way as before (see Fig. 10) or, if the friction is small enough, it can jump between potential wells before finally settling in one of the minimizers (see Fig. 11a). Even periodic trajectories around a point near a minimizer of $V_{\text{RWA}}(x)$ seem to exist (see Fig. 11b). It is an interesting open question to characterize and actually prove the existence of these periodic trajectories. In figures 10 and 11, $x(\tau)$ was computed numerically from (67) for several values of ξ , Γ , and Ω and for initial conditions such that the mirror starts from rest at a position where ω_0 coincides with one of the cavity resonance frequencies. Figure 9 also shows $x_{\text{RWA}}(\tau)$ calculated numerically from (68) with $a_0 = 1$ (the RWA regime). One can observe in Fig. 9 how the solution $x(\tau)$ of (67) tends to the solution $x_{\text{RWA}}(\tau)$ in the RWA regime as Ω increases. Notice that $x(\tau)$ with $\Omega = 10000$ is practically the same as $x_{\text{RWA}}(\tau)$. Also, we have obtained numerical evidence that the dynamics of the mirror are very sensitive to the value of Ω , since small changes in its value can lead to very different dynamics. This is illustrated in Fig. 11a) for values of Ω around 1000.

Using (58) and (67) it can be shown that sufficient conditions for (5) with $t \geq 0$ are the following:

$$2v_{\text{max}} \ll \Omega, \quad 4\Gamma v_{\text{max}} + 8f_{\text{RWA}}(x_{2n}) \ll \Omega^2, \quad (81)$$

with v_{max} an upper bound of $|x'(\tau)|$ for $\tau \geq 0$ and x_{2n} a maximizer of $f_{\text{RWA}}(x)$. If $\xi \gg 1$, then these reduce to the following:

$$2v_{\text{max}} \ll \Omega, \quad 4\Gamma v_{\text{max}} + 4\xi^2 \ll \Omega^2. \quad (82)$$

Here we used (35) to evaluate $f_{\text{RWA}}(x_{2n})$ for $\xi \gg 1$.

We now illustrate (82) for the parameters of Figs. 10 and 11a. In these figures $\xi = 50$, $v_{\text{max}} < 2.1$, $10^3 \leq \Omega$, and $\Gamma \leq 16$. Hence, $2v_{\text{max}} < 4.2 \ll 10^3 \leq \Omega$ and $4\Gamma v_{\text{max}} + 4\xi^2 \leq 10134.4 \ll 10^6 \leq \Omega^2$, so that (5) is satisfied for $t \geq 0$. Now we consider the case of Fig. 11b. The outside figure has $\Omega = 6$, $|x'(\tau)| \leq 1.6$ and $|x''(\tau)| \leq 100$ for $\tau \geq 0$. Using (58) it follows that (5) are not satisfied so $x(\tau)$ is not a physical solution

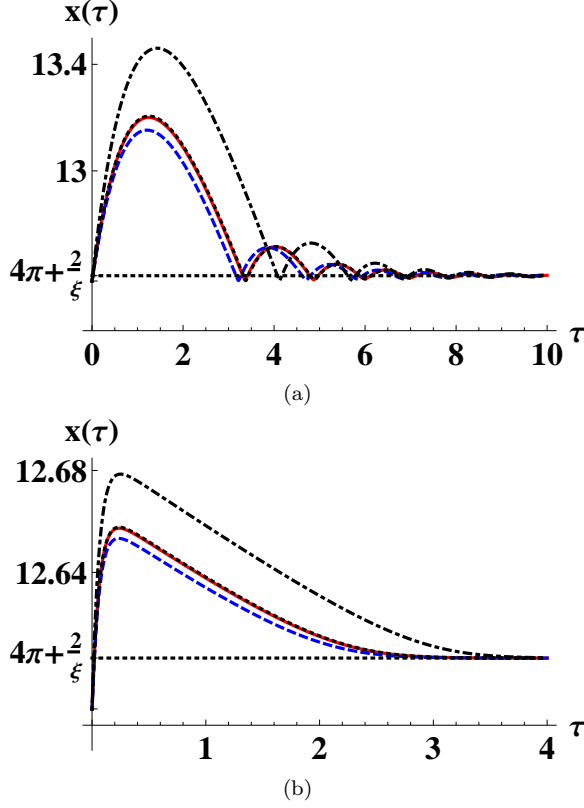


FIG. 10: (Color online) The figures show $x(\tau)$ computed numerically from (67) for $\Omega = 10000$ (red-solid line), $\Omega = 5000$ (blue-dashed line), and $\Omega = 1000$ (black-dot-dashed line). The figures also show $x_{\text{RWA}}(\tau)$ (black-dotted line) computed numerically from (68) with $a_0 = 1$ and the horizontal line $(4\pi + 1/\xi)$ showing approximately the position of the minimizer x_n^* of $V_{\text{RWA}}(x)$. In all figures $\xi = 50$ and the initial conditions are $x(0) = 4\pi + 1/\xi$ and $x'(0) = 0$. Fig. 10a has $\Gamma = 1$, while Fig. 10b has $\Gamma = 16$.

in the sense that the model is not applicable for all times. However, if one only considers $\tau \gg 1$, then $|x'(\tau)| \leq 0.25$ and $|x''(\tau)| \leq 1.7$ so that $|\dot{q}(t)/c| \leq 0.084$ and $|\ddot{q}(t)/(c\omega_0)| \leq 0.19$. Therefore, the model is approximately applicable for the steady-state periodic solution. The inside figure has the same problem, since the model is not applicable during the transient. For $\tau \gg 1$ it has $|x'(\tau)| \leq 0.094$ and $|x''(\tau)| \leq 1.5$ so that $|\dot{q}(t)/c| \leq 0.014$ and $|\ddot{q}(t)/(c\omega_0)| \leq 0.03$. Again, the model is approximately applicable for the steady-state periodic solution.

Finally we note that (40) can be used to solve (67) approximately if $\xi \gg 1$. We do not pursue this direction here.

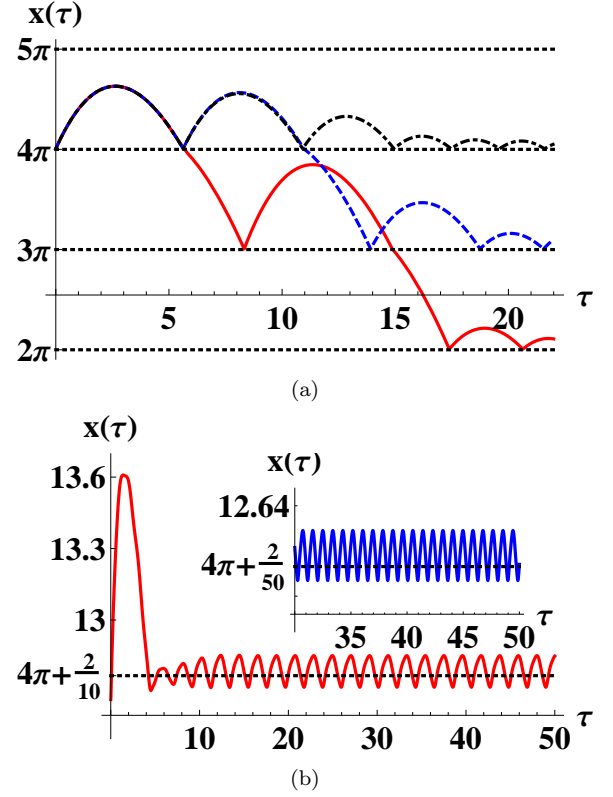


FIG. 11: (Color online) The figures show $x(\tau)$ computed numerically from (67) for several values of Γ and Ω and the initial conditions $x(0) = 4\pi + 1/\xi$ and $x'(0) = 0$. Figure 11a has $\xi = 50$, $\Gamma = 7/50$ and $\Omega = 1000$ (red-solid line), 1000.493 (blue-dashed line), and 1000.5 (black-dot-dashed line). The horizontal black-dotted lines at integer multiples of π indicate the beginning and the end of the wells of $V_{\text{RWA}}(x)$. The outer figure in 11b has $\xi = 10$, $\Gamma = 1$, and $\Omega = 6$. It also shows the constant black-dotted line at the minimizer $x_n^* \simeq (4\pi + 2/\xi)$ of $V_{\text{RWA}}(x)$. The inside figure in 11b has $\xi = 50$, $\Gamma = 1$, and $\Omega = 14.1$. It also shows the constant black-dotted line at the minimizer $x_n^* \simeq (4\pi + 2/\xi)$ of $V_{\text{RWA}}(x)$.

VI. INTRODUCTION OF A HARMONIC OSCILLATOR POTENTIAL

In the previous section it was shown that, in the high and low intensity limits and for $\xi \gtrsim 10$, the addition of friction leads to a final state in which the mirror is at rest at a position where ω_0 is very different from one of the cavity resonance frequencies. In experimental set-ups the movable mirror normally executes small oscillations around a position where ω_0 does coincide with one of the cavity resonance frequencies. In order to achieve this we assume in this section that the movable mirror is confined by a harmonic oscillator potential. The equation

governing the dynamics of the mirror is

$$\begin{aligned} & \frac{d^2 x}{d\tau^2}(\tau) + \Gamma \frac{dx}{d\tau}(\tau) + \omega_{\text{ho}}^2 [x(\tau) - x_E] \\ &= [1 + \cos(\Omega\tau)] f_{\text{RWA}}[x(\tau)] . \end{aligned} \quad (83)$$

Equation (83) is obtained by adding on the right-hand side of (8) the force $-\gamma\dot{q}(t) - k_{\text{ho}}[q(t) - q_E]$ and then using (25) to express the equation in terms of non-dimensional quantities. Here γ has units of Ns/m^3 and k_{ho} has units of N/m^3 . Also, $\Gamma = \gamma/(\Delta M_0)$, $\omega_{\text{ho}} = \sqrt{k_{\text{ho}}/(\Delta^2 M_0)}$, and $x_E = k_N^0 q_E$ are non-dimensional quantities.

In the rest of this section we assume that $x_E = x_{2n}$ for some $n \in \mathbb{Z}^+$, so that the harmonic oscillator potential is centred at a position where ω_0 coincides with one of the cavity resonance frequencies, see (13) and (35) and the definition of ξ in (25).

A. The limits of low and high field intensity

The limits of low and high field intensity are still defined by conditions (43) and (45), respectively. They allow us to eliminate the explicit time dependence in (83) to obtain

$$\frac{d^2 x}{d\tau^2}(\tau) + \Gamma \frac{dx}{d\tau}(\tau) + \omega_{\text{ho}}^2 [x(\tau) - x_E] = a_0 f_{\text{RWA}}[x(\tau)] , \quad (84)$$

with a_0 in (47). Notice that (84) can be written as

$$\frac{d^2 x}{d\tau^2}(\tau) + \Gamma \frac{dx}{d\tau}(\tau) = -\frac{d\mathcal{V}}{dx}[x(\tau)] , \quad (85)$$

where $\mathcal{V}(x)$ is the potential affecting the motion of the mirror. It is given by

$$\mathcal{V}(x) = a_0 V_{\text{RWA}}(x) + \frac{1}{2} \omega_{\text{ho}}^2 (x - x_E)^2 . \quad (86)$$

We now perform a phase space analysis of (84). The first order non-linear system associated with (84) is

$$\frac{d}{d\tau} \begin{pmatrix} x(\tau) \\ y(\tau) \end{pmatrix} = \mathbf{f}_{\text{ho}}[x(\tau), y(\tau)] . \quad (87)$$

Here $y(\tau) = x'(\tau)$ and

$$\mathbf{f}_{\text{ho}}(x, y) = \begin{pmatrix} y \\ -\Gamma y - \omega_{\text{ho}}^2 (x - x_E) + a_0 f_{\text{RWA}}(x) \end{pmatrix} . \quad (88)$$

Since $\nabla \cdot \mathbf{f}_{\text{ho}}(x, y) = -\Gamma < 0$ for all $x, y \in \mathbb{R}$, Bendixon's criterion (Theorem 1 in Section 3.9 of [31]) allows us to conclude that there are no closed orbits and no cycle-graphs in phase space. Moreover, the fixed points $(x_n^{\text{ho}}, y_n^{\text{ho}})$ of (87) are defined by

$$y_n^{\text{ho}} = 0 , \quad a_0 f_{\text{RWA}}(x_n^{\text{ho}}) = \omega_{\text{ho}}^2 (x_n^{\text{ho}} - x_E) . \quad (89)$$

Notice that x_n^{ho} is a critical point of the potential $\mathcal{V}(x)$, since the second equation in (89) can be written as $(d\mathcal{V}/dx)(x_n^{\text{ho}}) = 0$.

In the following we take x_n^{ho} to be the first (an possibly only) solution of the second equation in (89) located to the right of the maximizer $x_E = x_{2n}$ of $f_{\text{RWA}}(x)$ for each $n \in \mathbb{Z}^+$. Then x_n^{ho} is a minimizer of $\mathcal{V}(x)$ (this conclusion is immediate if one observes the graph of $V_{\text{RWA}}(x)$ in Fig. 3a and adds a harmonic oscillator potential centred at $x = n\pi + 1/\xi$). From (33) and (35) it follows that x_n^{ho} is located between a maximizer x_{2n} of $f_{\text{RWA}}(x)$ and a minimizer x_n^{**} of $V_{\text{RWA}}(x)$ if $\xi \gg 1$, that is, $x_{2n} \simeq n\pi + 1/\xi < x_n^{\text{ho}} < n\pi + 2/\xi \simeq x_n^{**}$ if $\xi \gg 1$.

The equation for x_n^{ho} in (89) can be solved to good approximation if $\xi \gtrsim 10$ and one uses (35) and the displaced Lorentzian approximation of $f_{\text{RWA}}(x)$ given in (37). One has to solve the cubic equation

$$u_n^3 + \frac{a_0}{2\omega_{\text{ho}}^2} u_n^2 + \frac{1}{\xi^4} u_n = \frac{a_0}{2\xi^2 \omega_{\text{ho}}^2} \left(1 - \frac{1}{\xi^2}\right) , \quad (90)$$

with $u_n = x_n^{\text{ho}} - (n\pi + 1/\xi)$. Using Descartes' rule of signs [32] it follows that (90) has exactly one positive real root (recall that we have defined x_n^{ho} to satisfy $x_n^{\text{ho}} > x_E$ so that $u_n > 0$). It can be calculated explicitly (using the Cardan's formulas [32] or symbolic calculations), but the expression is quite long. For this reason we have decided to omit it.

A linear stability analysis of (87) shows that the fixed point $(x_n^{\text{ho}}, y_n^{\text{ho}})$ is always an attractor. To prove this result one has to use that $a_0 f'_{\text{RWA}}(x_n^{\text{ho}}) < 0$, since $f_{\text{RWA}}(x)$ is strictly decreasing from its maximizer x_{2n} to x_n^{**} where it is zero and x_n^{ho} is located between them (see items 6 and 8 on page 5). In particular, $(x_n^{\text{ho}}, y_n^{\text{ho}})$ is a stable spiral (Theorem 4 of Section 2.10 of [31]) if

$$\left(\frac{\Gamma}{2}\right)^2 < \omega_{\text{ho}}^2 - a_0 f'_{\text{RWA}}(x_n^{\text{ho}}) . \quad (91)$$

On the other hand, it is a stable node (Theorem 4 of Section 2.10 of [31]) if the $<$ is replaced by \geq in (91). Notice that a typical value is $\Gamma/\omega_{\text{ho}} \sim 10^{-3}$ (see Appendix III), which gives a fixed point that is a stable spiral.

In general, the movable mirror tends to a minimizer or maximizer of $\mathcal{V}(x)$ as $\tau \rightarrow +\infty$. This follows from the Poincaré-Bendixon theory in \mathbb{R}^2 and from the facts that the energy of the movable mirror is always decreasing and that there are no closed orbits and cycle-graphs in phase space.

The approximation of $V_{\text{RWA}}(x)$ in (40) can be used to obtain an analytic approximation of the solution of (84), but this analytic approximation is not accurate. The reason is that the evolution predicted by the approximate $x(\tau)$ is qualitatively different and tends to 0 instead of x_n^{ho} if $\tau \rightarrow +\infty$. The displaced Lorentzian approximation for $f_{\text{RWA}}(x)$ could also be used in $V_{\text{RWA}}(x)$, but it seems that there is no explicit perturbative solution available (the perturbation parameter being $1/\xi$). Instead, we shall give an analytic approximation that qualitatively

describes the solution in the general case of (83) in the next subsection.

We now discuss the regime of validity of the model, that is, we establish sufficient conditions for (5) to be satisfied. We first consider the condition on the velocity of the mirror. From (85) it follows that the (non-dimensional) energy of the mirror is given by

$$E_{\text{ho}}[x(\tau), x'(\tau)] = \frac{1}{2} [x'(\tau)]^2 + \mathcal{V}[x(\tau)] , \quad (92)$$

and that it is a decreasing function of time

$$E_{\text{ho}}[x(\tau), x'(\tau)] = E_{\text{ho}}^0 - \Gamma \int_0^\tau d\tau' [x'(\tau')]^2 , \quad (93)$$

with $E_{\text{ho}}^0 \equiv E_{\text{ho}}[x(0), x'(0)]$ and $\tau \geq 0$. Hence, one can bound the velocity of the mirror using the bounds for $V_{\text{RWA}}(x)$ in (34) and (58), (92), and (93). One obtains

$$\left| \frac{\dot{q}(t)}{c} \right| \leq \frac{2}{\Omega} \sqrt{2E_{\text{ho}}^0 + a_0 \pi} \quad (t \geq 0). \quad (94)$$

Therefore, the first condition in (5) will be satisfied if Ω is much larger than the initial (non-dimensional) energy E_{ho}^0 of the mirror.

We now consider the condition on the acceleration of the mirror. Using the triangle inequality, the definition of a_0 , and (35), it follows from (58) and (84) that

$$\left| \frac{\ddot{q}(t)}{c\omega_0} \right| \leq \frac{8}{\Omega^2} f_{\text{RWA}}(x_{2n}) + \frac{2\Gamma}{\Omega} \left| \frac{\dot{q}(t)}{c} \right| + \frac{4\omega_{\text{ho}}^2}{\Omega^2} |x(\tau) - x_{\text{E}}| , \quad (95)$$

with $t \in \mathbb{R}$ and $\tau = \Delta t$. Therefore, the second condition in (5) will also be satisfied if Ω is large enough.

In particular, if $\xi \gg 1$ (say, $\xi \gtrsim 5$) and the movable mirror is confined to the interval $(n\pi, n\pi + 2/\xi)$ for $\tau \geq 0$, then (95) takes the form

$$\left| \frac{\ddot{q}(t)}{c\omega_0} \right| \lesssim \frac{4\xi^2}{\Omega^2} + \frac{4\Gamma}{\Omega^2} \sqrt{2E_{\text{ho}}^0 + \pi} + \frac{4\omega_{\text{ho}}^2}{\Omega^2 \xi} \quad (t \geq 0). \quad (96)$$

Here we used the bound in (94). Therefore, under the assumptions $\xi \gg 1$ and $x(\tau) \in (n\pi, n\pi + 2/\xi)$ for $\tau \geq 0$ the requirement on the acceleration of the mirror in (5) is satisfied if the condition on the velocity of the mirror in (94) holds and

$$\begin{aligned} 4\xi^2 &\ll \Omega^2 , \\ 2\Gamma &\ll \Omega , \\ 4\omega_{\text{ho}}^2 &\ll \Omega^2 \xi . \end{aligned} \quad (97)$$

Notice that the end points of the interval $(n\pi, n\pi + 2/\xi)$ are (approximately) consecutive maximizers and minimizers of $V_{\text{RWA}}(x)$ and that the non-dimensional position $x_{\text{E}} = x_{2n}$ where ω_0 coincides with one of the cavity resonance frequencies is located between them, see (32), (33), and (35).

To end this subsection we discuss the validity of the high and low intensity limit requirements in (43) and (45), respectively. First consider the case of the high intensity limit. From (94) and (95) it follows that (5) requires $\Omega \gg 1$, while the high intensity limit has $\Omega \ll 1$. Therefore, this again appears to be incompatible with the equations used in the model.

We now turn to the low intensity limit or RWA regime. In the following subsection it is shown that, after a transient, the solution of (83) approximately describes a harmonic oscillation of frequency Ω around the fixed point x_n^{ho} whose amplitude is estimated by

$$\frac{\xi^2 - 1}{2\sqrt{\Gamma^2 \Omega^2 + (\Omega^2 - \omega_{\text{ho}}^2)^2}} . \quad (98)$$

Hence, the amplitude of the oscillation will be small if

$$\frac{\xi^2 - 1}{2} \ll \sqrt{\Gamma^2 \Omega^2 + (\Omega^2 - \omega_{\text{ho}}^2)^2} . \quad (99)$$

We take (99) as a condition necessary for the RWA to be valid, since the amplitude of the steady state oscillations will be very small and the movable mirror will be found approximately at the fixed point x_n^{ho} just as predicted in the RWA regime. Since $\omega_{\text{ho}}/\Omega = (\Delta\omega_{\text{ho}})/(2\omega_0)$ with $\Delta\omega_{\text{ho}}$ the angular frequency of the harmonic oscillator potential and ω_0 the angular frequency of the field, one typically has $\omega_{\text{ho}}/\Omega \ll 1$. Also, $\Gamma/\Omega \ll 1$ because $\Gamma/\Omega = (\Delta\Gamma)/(2\omega_0)$ with $\Delta\Gamma$ the damping rate. Under these typical conditions (99) essentially reduces to $\Omega^2 \gg (\xi^2 - 1)/2$, since

$$\begin{aligned} \sqrt{\Gamma^2 \Omega^2 + (\Omega^2 - \omega_{\text{ho}}^2)^2} &= \Omega^2 \sqrt{\left(\frac{\Gamma}{\Omega}\right)^2 + \left[1 - \left(\frac{\omega_{\text{ho}}}{\Omega}\right)^2\right]^2} , \\ &\simeq \Omega^2 . \end{aligned} \quad (100)$$

One has (100) if one uses the typical values $\omega_{\text{ho}}/\Omega \sim 10^{-11}$ and $\Gamma/\Omega \sim 10^{-14}$ in Appendix III. Finally, notice that the RWA regime is compatible with the conditions in (5), since both essentially require Ω sufficiently large.

B. The intermediate case

In this subsection we treat the general case in (83). In all that follows we take $u(\tau) = x(\tau) - x_{\text{E}}$ for $\tau \geq 0$. We first give an analytic approximation of the solution in the case where the transparency of the movable mirror is small (that is, $\xi \gg 1$).

Assume that $\xi \gg 1$ and $|\xi^2 u(\tau)| \ll 1$ for $\tau \geq 0$. Then (83) can be approximated as

$$u''(\tau) + \Gamma u'(\tau) + \omega_{\text{ho}}^2 u(\tau) \simeq \frac{\xi^2 - 1}{2} [1 + \cos(\Omega\tau)] . \quad (101)$$

Here we used the displaced Lorentzian approximation to $f_{\text{RWA}}(x)$ in (37) and the assumptions $\xi \gg 1$ and

$|\xi^2 u(\tau)| \ll 1$ ($\tau \geq 0$) as follows

$$\begin{aligned} f_{\text{RWA}}[u(\tau) + x_E] &\simeq -\frac{1}{2} + \frac{\xi^2}{2} \frac{1}{[\xi^2 u(\tau)]^2 + 1}, \\ &\simeq -\frac{1}{2} + \frac{\xi^2}{2} \quad (\tau \geq 0). \end{aligned} \quad (102)$$

Equation (101) corresponds to a forced harmonic oscillator with damping. Its solution is

$$u(\tau) = u_{\text{st}}(\tau) + u_{\text{trans}}(\tau) \quad (\tau \geq 0), \quad (103)$$

with $u_{\text{st}}(\tau)$ the steady-state solution given by

$$\begin{aligned} u_{\text{st}}(\tau) &= \frac{\xi^2 - 1}{2\omega_{\text{ho}}^2} + \frac{\xi^2 - 1}{2} \frac{\cos(\Omega\tau - \theta)}{\sqrt{\Gamma^2\Omega^2 + (\Omega^2 - \omega_{\text{ho}}^2)^2}}, \\ \theta &= \cos^{-1} \left[\frac{\omega_{\text{ho}}^2 - \Omega^2}{\sqrt{\Gamma^2\Omega^2 + (\Omega^2 - \omega_{\text{ho}}^2)^2}} \right] \in (0, \pi), \end{aligned} \quad (104)$$

and $u_{\text{trans}}(\tau)$ a transient that decays exponentially to zero as $\tau \rightarrow +\infty$ (it is a solution of the homogeneous equation associated with (101)). One needs (103) to be consistent with the assumption $|\xi^2 u(\tau)| \ll 1$ for $\tau \geq 0$. Using that $\xi \gg 1$ one obtains

$$\begin{aligned} |\xi^2 u_{\text{st}}(\tau)| &\ll 1 \quad (\tau \geq 0) \\ \Leftrightarrow \xi^4 &\ll \min \left\{ \omega_{\text{ho}}^2, \sqrt{\Gamma^2\Omega^2 + (\Omega^2 - \omega_{\text{ho}}^2)^2} \right\}. \end{aligned} \quad (105)$$

The conditions on the right-hand side of (105) essentially say that ω_{ho} and either $\Gamma\Omega$ or $|\Omega^2 - \omega_{\text{ho}}^2|$ have to be sufficiently large so that the harmonic oscillator potential can confine the movable mirror to a small region around $x_E = x_{2n}$. We emphasize that the assumptions $\xi \gg 1$ and $|\xi^2 u(\tau)| \ll 1$ ($\tau \geq 0$) must be satisfied so that (103) is an accurate approximation to the solution of (83). Although these conditions are rather stringent, (103) qualitatively describes rather well the exact solution. We now show this through numerical calculations.

Figure 12a illustrates $u(\tau) = x(\tau) - x_E$ (red-solid line) calculated numerically from (83) once the transient term is negligible and compares it with $u_{\text{st}}(\tau)$ (blue-dashed line) given in (104), and the function $u_n + A\cos(\Omega\tau - \psi)$ (black-dotted line) with $A = 0.0438$, $\psi = 1.4$ ($\psi \simeq 1.57 = \theta$ with θ in (104)), and $u_n = x_n^{\text{ho}} - x_E = 0.00031$ with x_n^{ho} in (89). The parameters are $\xi = 10$, $\Omega = \omega_{\text{ho}} = 400$, and $\Gamma = 1$. Notice that the movable mirror behaves asymptotically as $u_n + A\cos(\Omega\tau - \psi)$ and that it oscillates in and out of the region $[-1/\xi^2, 1/\xi^2] = [-10^{-2}, 10^{-2}]$ where ω_0 coincides with a cavity resonance frequency (see (13)). Introducing units (that is, multiplying A by $1/k_N^0 = \lambda/(2\pi)$), it follows that the steady-state oscillations of the mirror have an amplitude approximately equal to $\lambda/(40\pi)$, which is on the order of 5nm for wavelengths in the optical regime. Also, the complete evolution from $\tau \geq 0$ (not shown) indicates that the movable

mirror behaves approximately as a resonantly forced and under-damped harmonic oscillator. The approximate solution in (103) allows one to identify this fact, but it reaches steady-state more slowly.

Figure 12b illustrates $u(\tau) = x(\tau) - x_E$ (red-solid line) calculated numerically from (83) and compares it with $u(\tau)$ (blue-dashed line) given in (103), and the function $u_F + A\cos(\Omega\tau - \psi)$ (black-dotted line) with $u_F = u_n - 2 \times 10^{-5}$, $A = 9.77 \times 10^{-4}$, and $\psi = 1.5$ ($\psi \simeq 1.57 = \theta$ with θ in (104)). The parameters are $\xi = 10$, $\Omega = \omega_{\text{ho}} = 100$, and $\Gamma = 400$ and the initial conditions are $u(0) = u'(0) = 0$. Observe that the movable mirror behaves asymptotically as $u_F + A\cos(\Omega\tau - \psi)$ and that it oscillates in the region $[-1/\xi^2, 1/\xi^2] = [-10^{-2}, 10^{-2}]$ where ω_0 coincides with a cavity resonance frequency. Introducing units (that is, multiplying A by $1/k_N^0 = \lambda/(2\pi)$), it follows that the steady-state oscillations of the mirror have approximately an amplitude of $\lambda/(2000\pi)$, which gives an amplitude on the order of 0.1nm for wavelengths in the optical regime. This last result is similar to that obtained in the experimental set up of [11]. The complete evolution from $\tau \geq 0$ now indicates that the movable mirror behaves approximately as a resonantly forced and over-damped harmonic oscillator. The approximate solution in (103) again allows one to identify this fact and reaches the steady-state (approximately) at the same time.

In both figures 12a and 12b the approximation in (104) qualitatively describes the evolution of the exact $u(\tau)$ for all $\tau \geq 0$. It identifies the frequency and approximately the phase and average position of the numerical solution, although the amplitude of the oscillations is overestimated. Moreover, (104) identifies that resonance occurs when $\Omega = \omega_{\text{ho}}$, since both (104) and our numerical calculations indicate that the amplitude of the oscillations is much smaller if ω_{ho} is very different from Ω . Using the definition of Ω in (25) one can rewrite the condition $\Omega = \omega_{\text{ho}}$ as $2\omega_0 = \Delta\omega_{\text{ho}}$. Hence, resonance occurs if the angular frequency $\Delta\omega_{\text{ho}}$ of the harmonic oscillator potential is twice the angular frequency of the field. Note that one is normally out of resonance, since one typically has $2\omega_0 \gg \Delta\omega_{\text{ho}}$ (from Appendix III a typical value is $\omega_{\text{ho}}/\Omega \sim 10^{-11}$ for field frequencies in the optical regime).

Finally, in both cases the steady-state solution behaves asymptotically as $u(\tau) \simeq u_0 + A\cos(\Omega\tau - \psi)$, where u_0 is a point near $x_n^{\text{ho}} - x_E$.

To end this subsection we comment on the validity of the model, that is, we discuss if (5) are satisfied. In a similar way as in the previous subsection it can be shown from (83) that (95) still holds. The problem is that there is no direct way to bound the velocity of the mirror, since energy is no longer conserved. Nevertheless, using the approximate $u(\tau)$ in (103) one can obtain the following estimate:

$$\left| \frac{\dot{q}(t)}{c} \right| \lesssim \frac{|\xi^2 - 1|}{\sqrt{\Gamma^2\Omega^2 + (\Omega^2 - \omega_{\text{ho}}^2)^2}} \quad (\tau \gg 1). \quad (106)$$

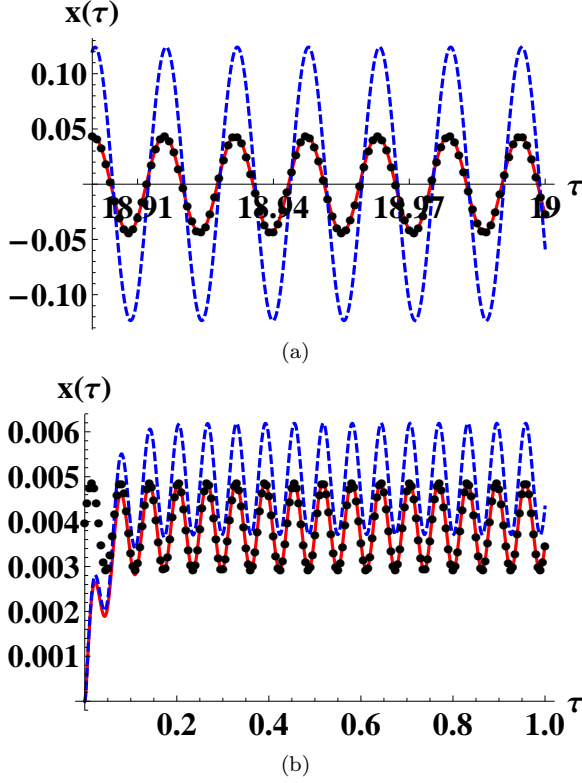


FIG. 12: (Color online) The figures show $u(\tau) = x(\tau) - x_E$ (red-solid line) calculated numerically from (83) and the function $u_0 + A\cos(\Omega\tau - \psi)$ (black-dotted line) for $\xi = 10$ and $\Omega = \omega_{ho}$. Figure 12a also shows $u_{st}(\tau)$ (blue-dashed line) given in (104) and has $\Gamma = 1$, $\Omega = 400$, $A = 0.0438$, $\psi = 1.4$, and $u_0 = u_n = x_n^{ho} - x_E = 0.00031$. Figure 12b also shows $u(\tau)$ given in (103) and has $\Gamma = 400$, $\Omega = 100$, $A = 9.77 \times 10^{-4}$, $\psi = 1.5$, and $u_0 = u_n - 2 \times 10^{-5}$. Here x_n^{ho} is defined in (89).

From (95) and (106) it follows that (5) will be satisfied if Ω is sufficiently large and, for example, $\Omega \gg \omega_{ho}$, that is, the field is far off resonance with the frequency of the harmonic oscillator potential. Notice that this condition is satisfied for the typical value $\omega_{ho}/\Omega \sim 10^{-11}$ (see Appendix III).

We now illustrate (95) and (106) with the parameters of Fig. 11. The numerical solution in Fig. 12a has $|x'(\tau)| \leq 20$ and $|x''(\tau)| \leq 8000$ for $\tau \geq 0$. Substituting these values and the value $\Omega = 400$ from Fig. 12a in (58) one obtains $|\dot{q}(t)/c| \leq 0.1$ and $|\ddot{q}(t)/(c\omega_0)| \leq 1/5$, so that (5) are roughly satisfied. Therefore, the model of Sec. II is roughly applicable. If one substitutes the parameters of Fig. 12a in the right-hand side of (95) and (106), then one obtains $|\dot{q}(t)/c| \leq 1/4$ and $|\ddot{q}(t)/(c\omega_0)| \lesssim 1/5$, so that (95) and (106) correctly reflect the fact that the model is roughly applicable. On the other hand, the numerical solution in Fig. 12b has $|x'(\tau)| \leq 0.21$ and $|x''(\tau)| \leq 100.1$ for $\tau \geq 0$. Substituting these values and the value $\Omega = 100$ from

Fig. 12b in (58) one obtains $|\dot{q}(t)/c| \lesssim 4.2 \times 10^{-3}$ and $|\ddot{q}(t)/(c\omega_0)| \lesssim 4 \times 10^{-2}$, so that that (5) are satisfied. Therefore, the model of Sec. II is applicable in this case. If one substitutes the parameters of Fig. 12b in the right-hand side of (95) and (106), then one obtains $|\dot{q}(t)/c| \leq 1/400$ and $|\ddot{q}(t)/(c\omega_0)| < 0.1$. Hence, (95) and (106) reflect the fact that the model is applicable.

VII. CONCLUSIONS

In this article we considered one of the paradigmatic models in optomechanics: a one-dimensional cavity composed of a perfect and fixed mirror and of a movable mirror with non-zero transparency subject to the radiation pressure of a single-mode electromagnetic field. Our approach differs from most of the articles in that we considered the exact modes of the whole system and did not divide them into modes of the cavity and modes outside of it as if the mirrors composing the cavity were perfect. This allowed us to conclude that the radiation pressure force of the single-mode field is derived from a periodic potential with period half the wavelength of the field and that the dynamics of the mirror due to radiation pressure are determined by the mirror approaching or withdrawing from a *resonance position* where the frequency of the field coincides with one of the cavity resonance frequencies. Moreover, there is only one resonance position in each well of the potential.

Special attention was given to establishing and verifying conditions that determine when the equations used to describe the physical system are accurate approximations to the exact Maxwell-Newton equations. These amount to asking that the velocity and acceleration of the mirror be small enough so that the electromagnetic field evolves as if the mirror were instantaneously fixed. We identified three regimes: the low intensity or rotating-wave-approximation (RWA) regime, the high intensity regime, and the intermediate regime. The first one occurs when the frequency of the field is much larger than 1 over the characteristic time-scale of the movable mirror, the second when the former is much smaller than the latter, and the third treats the values in between. We found that the RWA regime is a natural setting for the equations, while the intermediate regime is compatible with them for a certain range of parameters (namely, Ω not too small). The high intensity regime appears to be incompatible with the equations used, since the movable mirror can be subject to large accelerations in this case.

The introduction of the radiation pressure potential gave rise to an intuitive physical understanding of the dynamics of the movable mirror. In the RWA regime and when only radiation pressure is considered, the movable mirror has constant energy and can have either a bounded or unbounded trajectory where it accelerates as it approaches a minimizer and decelerates as it approaches a maximizer of the radiation pressure potential. In the case of a bounded trajectory, the movable mirror

is bound to one of the potential wells and executes a periodic trajectory around one of the minimizers of the radiation pressure potential. The consideration of the exact modes of the whole system allowed us to explain this trajectory as follows. As the mirror approaches the resonance position, the cavity field increases and exerts a radiation pressure that surpasses the one exerted by the field outside the cavity and that pushes the mirror away from the resonance position. As the mirror withdraws from the resonance position, the cavity field is emptied and the field outside exerts a larger force that pushes the mirror back to the resonance position. This process repeats itself over and over giving rise to the periodic trajectory of the mirror. Outside the RWA regime the dynamics of the mirror are much more complex since the mirror can jump between potential wells.

In the RWA regime and when the movable mirror is also subject to friction linear in the velocity, the movable mirror continually losses energy and eventually tends to the position of a minimizer (or maximizer) of the radiation pressure potential. Since this position is very different from the resonance position, the cavity field is emptied. Outside the RWA regime the dynamics are much more complex, since the movable mirror can jump between wells of the radiation pressure potential before settling in one of its minimizers (or maximizers). For some values of the parameters there is numerical evidence that the mirror can even execute periodic oscillations around one the minimizers. It is an interesting problem to prove the existence and to determine the conditions necessary for this type of behavior.

In the RWA regime and when the movable mirror is subject both to friction and to a harmonic oscillator potential centred at a resonance position, the movable mirror always tends to a minimizer (or maximizer) of the sum of the harmonic oscillator and radiation pressure potentials. Outside the RWA regime and after a transient, the movable mirror settles in a harmonic oscillation of frequency 2 times the frequency of the field and around an aforementioned minimizer. Moreover, there is resonance in the amplitude if the frequency of the harmonic oscillator is equal to two times the frequency of the field.

We believe that the approach that we have taken in this article and the results that we have obtained lead to a very good understanding of the radiation pressure of a single-mode field and of the regime of validity of the equations used to describe physical phenomena in optomechanics. In future work we will consider both the case of a field composed of multiple modes and the case where the motion of the movable mirror is quantized.

ACKNOWLEDGEMENTS

We thank Pablo Barberis-Blostein, Marc Bienert, and Christian Gerard for fruitful discussions. L. O. Castaños wishes to thank the Universidad Nacional Autónoma de México for support. Research partially supported by

CONACYT under Project CB-2008-01-99100.

* E-mail: LOCCJ@yahoo.com

+ Fellow, Sistema Nacional de Investigadores. E-mail: weder@unam.mx

APPENDIX I

In this appendix we calculate the maximizers and minimizers of $L_k(q)$ given in (11) as a function of $q \geq 0$ for fixed $k > 0$ and $\chi_0 > 0$.

First observe from the definition of $L_k(q)$ in (11) that

$$L_k(q) = \sqrt{\frac{2}{\pi}} \left[1 + \frac{(4\pi\chi_0 k)^2}{2} - (4\pi\chi_0 k) \sin(2kq) - \frac{(4\pi\chi_0 k)^2}{2} \cos(2kq) \right]^{-1/2}. \quad (107)$$

It then follows that

$$\frac{dL_k}{dq}(q_n) = 0 \Leftrightarrow \tan(2kq_n) = \frac{2}{4\pi\chi_0 k}. \quad (108)$$

In the following assume that

$$4\pi\chi_0 k \gg 1. \quad (109)$$

From (12) it follows that (109) implies that the transparency of the movable mirror is very small.

Using (109) it follows that a first approximation $q_n \simeq n\pi/(2k)$ with $n \in \mathbb{Z}^+$ (\mathbb{Z}^+ is the set of non-negative integers) is obtained by neglecting the term $2/(4\pi\chi_0 k)$ on the right of (108). Using Newton's method [33] one can obtain a better approximation of q_n . After one iteration it follows that

$$q_n \simeq \frac{1}{2k} \left(n\pi + \frac{2}{4\pi\chi_0 k} \right) \quad (n \in \mathbb{Z}^+). \quad (110)$$

Evaluating $d^2 L_k(q)/dq^2$ at $q = q_n$ given in (110) it follows that q_{2n} (q_{2n-1}) are maximizers (minimizers) of $L_k(q)$. Moreover, using the approximate values of q_n given in (110) and approximating $\sin[2/(4\pi\chi_0 k)]$ and $\cos[2/(4\pi\chi_0 k)]$ by their Taylor polynomials of degree 4 centred at 0, it follows from (107) that

$$\begin{aligned} L_k(q_{2n}) &\simeq \sqrt{\frac{2}{\pi}} (4\pi\chi_0 k), \\ L_k(q_{2n+1}) &\simeq \sqrt{\frac{2}{\pi}} \left(\frac{1}{4\pi\chi_0 k} \right) \times \\ &\quad \times \left[1 + \frac{2}{(4\pi\chi_0 k)^2} - \frac{1}{(4\pi\chi_0 k)^4} \right]^{-1/2}, \\ &\simeq \sqrt{\frac{2}{\pi}} \left(\frac{1}{4\pi\chi_0 k} \right), \end{aligned} \quad (111)$$

for each $n \in \mathbb{Z}^+$. In the approximate equality of $L_k(q_{2n})$ and the last approximate equality of $L_k(q_{2n+1})$ terms of

order $1/(4\pi\chi_0 k)^2$ and smaller have been neglected with respect to 1. Also, using (110) it follows that the distance between consecutive maximizers is $q_{2(n+1)} - q_{2n} \simeq \pi/k$ with $n \in \mathbb{Z}^+$, which corresponds to half the wavelength $\lambda/2 = \pi/k$. Notice that the maximum (minimum) of $L_k(q)$ increases (decreases) as the transparency of the mirror decreases.

To end this appendix we show that $L_k(q)^2$ can be approximated by a Lorentzian in a neighborhood of each maximizer q_{2n} and we comment on the relation of q_{2n} with the cavity resonance frequencies.

In the following we take

$$\begin{aligned} \xi &\equiv 4\pi\chi_0 k, \\ v &\equiv k(q - q_{2n}) \quad \text{for some fixed } n \in \mathbb{Z}^+, \\ f_0(q) &\equiv 1 + \frac{\xi^2}{2} - \xi \sin(2kq) - \frac{\xi^2}{2} \cos(2kq). \end{aligned} \quad (112)$$

Approximating $f_0(q)$ by its second order Taylor polynomial centred at q_{2n} , approximating q_{2n} by the value on the right-hand side of (110), approximating $\sin(2/\xi)$ and $\cos(2/\xi)$ by their fourth order Taylor polynomials centred at 0, simplifying, and then neglecting terms of order $1/\xi^2$ and smaller with respect to 1 it follows that

$$f_0(q) \simeq \frac{1}{\xi^2} + \xi^2 v^2. \quad (113)$$

Substituting (113) in the formula for $L_k(q)$ one obtains the following Lorentzian approximation to $L_k(q)^2$:

$$L_k(q)^2 = \frac{2}{\pi} f_0(q)^{-1} \simeq \frac{2}{\pi \xi^2} \left(\frac{1}{v^2 + \frac{1}{\xi^4}} \right). \quad (114)$$

Recall that we have been working under the assumption given in (109). Therefore, the approximation in (110) is accurate, the fourth order Taylor polynomials of $\sin(2/\xi)$ and $\cos(2/\xi)$ are accurate approximations of the corresponding functions, and neglecting terms of order $1/\xi^2$ with respect to 1 is also an accurate approximation. It then follows that the Lorentzian approximation to $L_k(q)^2$ will be accurate when the error in approximating $f_0(q)$ by its second order Taylor polynomial centred at q_{2n} is small, that is, when

$$\left| \frac{1}{2} f_0''(q_{2n}) \left(\frac{v}{k} \right)^2 \right| \gg \left| \frac{1}{3!} f_0'''(q^{(0)}) \left(\frac{v}{k} \right)^3 \right|, \quad (115)$$

with $q^{(0)}$ in the open interval whose end points are q and q_{2n} .

Simplifying (115) and bounding $|f_0'''(q^{(0)})|$ one concludes that the Lorentzian approximation to $L_k(q)^2$ is accurate if (109) holds and

$$|v| \ll \frac{3}{2}. \quad (116)$$

Using the definition of v in (112) one obtains that (116) can be written as $|q - q_{2n}| \ll 3/(2k)$. Since $|q_{2n\pm 1} -$

$q_{2n}| = \pi/(2k)$ (see (110)), it follows that (109) and (116) simply state that the Lorentzian approximation to $L_k(q)^2$ is accurate if the transparency of the movable mirror is small and one restricts to an interval around q_{2n} whose endpoints are not near the minimizers $q_{2n\pm 1}$ of $L_k(q)$.

In the rest of this appendix assume that the condition in (116) is also satisfied. Then the Lorentzian approximation of $L_k(q)^2$ in (114) is accurate and it has a half-width-at-half-maximum (HWHM) of $1/\xi^2$. Notice that the value of the HWHM is independent of the value of n in q_{2n} and it decreases as the transparency of the mirror decreases. Moreover, observe that $v \in [-1/\xi^2, 1/\xi^2]$ if and only if $kq \in [kq_{2n} - 1/\xi^2, kq_{2n} + 1/\xi^2]$.

First assume that $kq \in [kq_{2n} - 1/\xi^2, kq_{2n} + 1/\xi^2]$. From (111) and (114) it follows that $L_k(q)$ is very large and the mode $V_k(x, q)$ in (10) is much larger inside the cavity (that is, $0 \leq x \leq q = q_{2n}$) than outside of it (that is, $q = q_{2n} < x$). Therefore, $\omega = ck$ coincides with one of the cavity resonance frequencies for these values of q .

Now assume that $kq \notin [kq_{2n} - 1/\xi^2, kq_{2n} + 1/\xi^2]$ for all $n \in \mathbb{Z}^+$. Then $L_k(q)$ is very small and the mode $V_k(x, q)$ in (10) is much smaller inside the cavity than outside of it. In this case $\omega = ck$ is very different from any of the cavity resonance frequencies.

APPENDIX II

In this appendix we derive various properties of the force $f_{\text{RWA}}(x)$ and the potential $V_{\text{RWA}}(x)$ given respectively in (28) and (31).

First consider the function

$$f(x) = 1 + \xi^2 \sin^2(x) - \xi \sin(2x) \quad (x \geq 0). \quad (117)$$

Notice that $f(x) > 0$ for all $x \in \mathbb{R}$. In the following assume that

$$\xi \gg 1. \quad (118)$$

From (26) it follows that the condition in (118) implies that the transparency of the movable mirror is very small.

From (117) it follows that

$$f'(x_n) = 0 \Leftrightarrow \tan(2x_n) = \frac{2}{\xi}. \quad (119)$$

A first approximation to the solutions x_n of the equation on the right of (119) can be obtained by using (118) to neglect the term $2/\xi$. One obtains $x_n \simeq n\pi/2$ with $n \in \mathbb{Z}^+$ and \mathbb{Z}^+ the set of non-negative integers. Using Newton's method [33] one can obtain a second more accurate approximation. After one iteration the result is

$$x_n \simeq n\frac{\pi}{2} + \frac{1}{\xi} \quad (n \in \mathbb{Z}^+). \quad (120)$$

Evaluating numerically the solutions of the equation on the left of (119) one finds that the values on the right in (120) are a very good approximation to the corresponding

exact critical point x_n if $\xi \geq 5$, since the relative error $|x_n - (n\pi/2 + 1/\xi)|/|x_n|$ is less than 10^{-2} if $\xi \geq 5$ and less than 10^{-3} if $\xi \geq 10$. Also notice that x_n coincides with kq_n in (110).

Evaluating $f''(x)$ at $x = x_n$ and using the approximation in (120) one obtains that x_{2n+1} (x_{2n}) are maximizers (minimizers) of $f(x)$. Since

$$f_{\text{RWA}}(x) = -\frac{1}{2} \left[1 - \frac{1}{f(x)} \right], \quad (121)$$

it follows that x_{2n} (x_{2n+1}) is a maximizer (minimizer) of $f_{\text{RWA}}(x)$ for each $n \in \mathbb{Z}^+$. Substituting (120) in $f_{\text{RWA}}(x)$ and preserving only terms of order ξ^2 and 1 (terms of order ξ^{-2} and smaller are neglected) it follows that

$$f_{\text{RWA}}(x_n) \simeq \begin{cases} \frac{\xi^2}{2} - \frac{7}{18} & \text{if } n \text{ is even,} \\ -\frac{1}{2} & \text{if } n \text{ is odd.} \end{cases} \quad (122)$$

In a similar way, one can also calculate the zeros of $f_{\text{RWA}}(x)$ using (118) and Newton's method. One obtains that $f_{\text{RWA}}(x) = 0$ if and only if $x = x_n^*$ or $x = x_n^{**}$ with

$$x_n^* = n\pi \quad \text{and} \quad x_n^{**} \simeq n\pi + \frac{2}{\xi} \quad (n \in \mathbb{Z}^+). \quad (123)$$

We remark that $n\pi$ is an exact zero of $f_{\text{RWA}}(x)$.

From (120), (122), and (123) it follows that $f_{\text{RWA}}(x)$ has maximizers located at x_{2n} ($n \in \mathbb{Z}^+$) and that

$$x_n^* = n\pi \leq x_{2n} \simeq n\pi + \frac{1}{\xi} \leq x_n^{**} \simeq n\pi + \frac{2}{\xi}. \quad (124)$$

Notice that the length $2/\xi$ of the interval in (124) becomes smaller as the transparency of the movable mirror decreases.

We now show how $f_{\text{RWA}}(x)$ can be approximated by a Lorentzian in a neighborhood of each of its maximizers x_{2n} . In the following take $n \in \mathbb{Z}^+$ and

$$u = x - \left(n\pi + \frac{1}{\xi} \right). \quad (125)$$

Using the Taylor series expansion of $\tan(x)$ centred at 0 it follows that

$$\tan(x) \simeq u + \frac{1}{\xi}. \quad (126)$$

The right-hand side of (126) will be an accurate approximation of the left-hand side if the first correction to the right-hand side is much smaller than $(u + \xi^{-1})$, that is, if $1 \gg 3^{-1}(u + \xi^{-1})^2$. Using (126) in the expression (31) for $V_{\text{RWA}}(x)$ and neglecting 1 with respect to ξ^2 in the factor $(1 + \xi^2)$ (recall that we have been working all this time under the assumption in (118)) it follows that

$$V_{\text{RWA}}(x) \simeq \frac{1}{2} \left[u + \left(n\pi + \frac{1}{\xi} \right) \right] - \frac{1}{2} [\tan^{-1}(\xi) + n\pi]$$

$$-\frac{1}{2} \tan^{-1}(\xi^2 u), \quad (127)$$

for $(2n-1)\pi/2 \leq x \leq (2n+1)\pi/2$ and $x \geq 0$. Taking the derivative with respect to x one obtains that

$$f_{\text{RWA}}(x) \simeq -\frac{1}{2} + \frac{1}{2\xi^2} \frac{1}{u^2 + \xi^{-4}}, \quad (128)$$

for $(2n-1)\pi/2 < x < (2n+1)\pi/2$ and $x > 0$ and u given in (125). One should expect the approximations in (127) and in (128) to be accurate if $1 \gg 3^{-1}(u + \xi^{-1})^2$ and $\xi \gg 1$. Calculating numerically the relative error between $f_{\text{RWA}}(x)$ and the approximation in (128) we found that the displaced Lorentzian approximates $f_{\text{RWA}}(x)$ well if $\xi \gtrsim 10$ and $-1/\xi < u < 1/\xi$ (that is, x is not very near the points where $f_{\text{RWA}}(x)$ is zero). From (128) it follows that the maximizer $x_{2n} \simeq (n\pi + \xi^{-1})$ of $f_{\text{RWA}}(x)$ has a half-width-at-half-maximum (approximately) equal to $1/\xi^2$. Indeed, it can be shown that

$$f_{\text{RWA}} \left(n\pi + \frac{1}{\xi} \pm \frac{1}{\xi^2} \right) \simeq \frac{\xi^2}{4} \simeq \frac{1}{2} f_{\text{RWA}}(x_{2n}). \quad (129)$$

The first approximation in (129) was obtained by preserving only the terms of order ξ^2 (terms of order ξ and smaller were neglected). For the second approximation we used (122).

From (30) one has $f_{\text{RWA}}(x) = -(dV_{\text{RWA}}/dx)(x)$. Hence, the critical points x_n^* and x_n^{**} of $V_{\text{RWA}}(x)$ are given in (123). Evaluating $(d^2V_{\text{RWA}}/dx^2)(x)$ at the critical points it follows that $x_n^* = n\pi$ ($x_n^{**} \simeq n\pi + 2/\xi$) are maximizers (minimizers) of $V_{\text{RWA}}(x)$. Moreover, for $n \in \mathbb{Z}^+$ one has

$$V_{\text{RWA}}(n\pi) = 0,$$

$$V_{\text{RWA}} \left(n\pi + \frac{2}{\xi} \right) \simeq -\tan^{-1}(\xi). \quad (130)$$

The first equality in (130) is exact, while the second is obtained by neglecting terms of order $1/\xi$ and smaller. Also, one has $V_{\text{RWA}}(n\pi + 2/\xi) \rightarrow -\pi/2$ if $\xi \rightarrow +\infty$. Notice that $V_{\text{RWA}}(n\pi) = 0$ so that $V_{\text{RWA}}(x)$ has a jump discontinuity at $n\pi$ in the limit $\xi \rightarrow +\infty$.

To end this appendix we drop the assumption $\xi \gg 1$ in (118) and we prove that $-\pi/2 < V_{\text{RWA}}(x) \leq 0$ for all $x \geq 0$.

First observe that the inequality $V_{\text{RWA}}(x) \leq 0$ for all $x \geq 0$ is obtained by noticing that $V_{\text{RWA}}(x)$ is a continuous periodic function with maximizers x_n^* given in (123) and with maximum values given in (130).

We now consider the lower bound $-\pi/2 < V_{\text{RWA}}(x)$ for all $x \geq 0$. From the definition of $V_{\text{RWA}}(x)$ in (31) and from (130) one has

$$\begin{aligned} V_{\text{RWA}} \left[(2m+1) \frac{\pi}{2} \right] &= -\frac{1}{2} \tan^{-1}(\xi) \geq -\frac{\pi}{4}, \\ V_{\text{RWA}}(m\pi) &= 0, \end{aligned} \quad (131)$$

for each $m \in \mathbb{Z}^+$. Therefore, all that remains is to show that $-\pi/2 < V_{\text{RWA}}(x)$ for all $x \geq 0$ with $x \neq m\pi$, $(2m+1)\pi/2$ and $m \in \mathbb{Z}^+$.

To see this fix $x \geq 0$ and $m \in \mathbb{Z}^+$ with $(2m-1)\pi/2 < x < (2m+1)\pi/2$ and $x \neq m\pi$. Then one can consider $V_{\text{RWA}}(x)$ to be a function of ξ and we write $V_{\text{RWA}}(x, \xi)$ for clarity. From the definition of $V_{\text{RWA}}(x)$ in (31) one has for $\xi \geq 0$ that

$$\frac{\partial}{\partial \xi} V_{\text{RWA}}(x, \xi) = -\frac{1}{2} \frac{1}{\xi^2 + 1} - \frac{1}{2} \frac{2\xi \tan(x) - 1}{[(1 + \xi^2)\tan(x) - \xi]^2 + 1}. \quad (132)$$

It then follows that

$$\frac{\partial}{\partial \xi} V_{\text{RWA}}(x, \xi) < 0 \quad \text{for } \xi \geq 0. \quad (133)$$

Hence, $V_{\text{RWA}}(x, \xi)$ is a strictly decreasing function of $\xi \geq 0$ and one has

$$\lim_{\xi \rightarrow +\infty} V_{\text{RWA}}(x, \xi) < V_{\text{RWA}}(x, \xi). \quad (134)$$

Also, using $\Theta(y)$ to denote the Heaviside step function equal to 1 (0) if $y > 0$ ($y < 0$), it can be shown that

$$\lim_{\xi \rightarrow +\infty} V_{\text{RWA}}(x, \xi) = \frac{x}{2} - m\frac{\pi}{2} - \frac{\pi}{2}\Theta[\tan(x)] > -\frac{\pi}{2}, \quad (135)$$

From (134) and (135) one obtains that $-\pi/2 < V_{\text{RWA}}(x, \xi)$. Therefore, $-\pi/2 < V_{\text{RWA}}(x)$ for all $x \geq 0$.

APPENDIX III

In this appendix we take the parameters from [14] and adapt them to our system. It is important to note that the experimental set-up of [14] is dominated by bolometric forces (that is, light absorption deflecting the movable mirror), while the system we are studying only takes into consideration radiation pressure. The intention is to use the parameters of [14] so that one can get an idea of the order of magnitude of the quantities involved in the model.

The movable mirror of [14] is a gold-coated atomic force microscopy cantilever of length $L = 223\mu\text{m}$, width $W = 22\mu\text{m}$, thickness $\delta_{\text{thick}} = 512\text{ nm}$, and a spring constant $K_{\text{ho}} = 0.01\text{ N/m}$. Here we have added to δ_{thick} the thickness of the gold layer. For a wavelength of $\lambda = 633\text{ nm}$ the movable mirror has a reflectivity of 0.91. Moreover, the cantilever's fundamental mechanical mode has a frequency of $\omega_1 = 2\pi \times 8.7\text{ kHz}$ and a damping rate of $\Gamma_1 = 30\text{ Hz}$.

From the parameters above it follows that the effective mass M of the gold-coated cantilever is

$$M = \frac{K_{\text{ho}}}{\omega_1^2} = 3.3 \times 10^{-12}\text{ kg}. \quad (136)$$

Even if the set-up of [14] were dominated by radiation pressure, the model of this article would not be applicable since $\delta_{\text{thick}} \sim \lambda$. To apply the model one would need $\delta_{\text{thick}} \ll \lambda$, say $\delta_{\text{thick}} = 10^{-2}\lambda = 6.33\text{ nm}$. Therefore, we take the mass per unit area M_0 to be the value that would be obtained if the gold-coated cantilever had uniform mass density and thickness 100 times smaller, that is,

$$M_0 = \frac{1}{100} \frac{M}{LW} = 6.8 \times 10^{-6} \frac{\text{kg}}{\text{m}^2}, \quad (137)$$

From the parameters above we take

$$k_N^0 = \frac{2\pi}{\lambda} = \frac{2\pi}{633} \times 10^9\text{ m}^{-1}, \quad \omega_0 = ck_N^0 \simeq 3 \times 10^{15}\text{ s}^{-1}, \quad (138)$$

for the wave-number and angular frequency of the single-mode field. Using (137) and (138) it follows from (25) that

$$\Delta = 3.8 \times 10^{12} \times g_0, \quad \Omega = \frac{1562.6}{g_0}. \quad (139)$$

Here g_0 and Δ have units of $\text{N}^{1/2}$ and $1/\text{s}$, respectively, while Ω is non-dimensional. Using (139) one then obtains the non-dimensional quantities

$$\Gamma = \frac{\Gamma_1}{\Delta} = \frac{7.9 \times 10^{-12}}{g_0}, \quad \omega_{\text{ho}} = \frac{\omega_1}{\Delta} = \frac{1.4 \times 10^{-8}}{g_0}. \quad (140)$$

From (139) and (140) it follows that

$$\frac{\Gamma}{\Omega} \sim 10^{-14}, \quad \frac{\omega_{\text{ho}}}{\Omega} \sim 10^{-11}, \quad \frac{\Gamma}{\omega_{\text{ho}}} \sim 10^{-3}. \quad (141)$$

According to [22] the transmissivity T of the *delta*-mirror is related to $\xi = 4\pi\chi_0 k_N^0$ in (25) by

$$T = \frac{1}{1 + \left(\frac{\xi}{2}\right)^2} \Leftrightarrow \xi = 2\sqrt{\frac{R}{1-R}}. \quad (142)$$

Here we used that $R + T = 1$ with R the reflectivity. Using the value $R = 0.91$ given above one obtains that $\xi = 6.4$. Also, $\xi = 50$ if and only if $R = 0.9984$.

All that remains is to give a typical value for g_0 . We determine this by calculating the flux of energy per unit time into the cavity. Using the parameters above we take the cavity to be given by the box

$$V = [0, q(t)] \times \left[-\frac{L}{2}, \frac{L}{2}\right] \times \left[-\frac{W}{2}, \frac{W}{2}\right]. \quad (143)$$

Moreover, the plane $\{q(t) + \eta\} \times [-\frac{L}{2}, \frac{L}{2}] \times [-\frac{W}{2}, \frac{W}{2}]$ with $0 < \eta \ll 1$ is denoted by P_η .

From (2) and (24) it follows that the right-hand limit of the Poynting vector as $x \downarrow q(t)$ is given by

$$\mathbf{S}[q(t)+, t] = \lim_{x \rightarrow q(t)+} \frac{c}{4\pi} \mathbf{E}(x, t) \times \mathbf{B}(x, t),$$

$$= g_0^2 \frac{\omega_0^2}{4\pi c} L_{k_N^0} [q(t)]^2 \sin(2\omega_0 t) \times \{ \sin[2k_N^0 q(t)] - 2\xi \sin^2[k_N^0 q(t)] \} \mathbf{x} , \quad (144)$$

with \mathbf{x} the unit vector in the direction of the positive x -axis. In calculating the Poynting vector we neglected terms proportional to $\dot{q}(t)/c$.

The flux of energy per unit time into the cavity is then

$$P(t) = \lim_{\eta \rightarrow 0^+} \int_{P_\eta} \mathbf{S}(x, t) \cdot (-\mathbf{x}) da , \\ = -LW \mathbf{S}[q(t)+, t] \cdot \mathbf{x} . \quad (145)$$

Now assume that $k_N^0 q(t) \simeq n\pi + 1/\xi$ with $\xi = 4\pi\chi_0 k_N^0 \gtrsim 5$ so that ω_0 coincides with one of the cavity resonance frequencies (see Appendix I). It follows from (111), (144), and (145) that

$$P(t) \simeq LW \frac{g_0^2 \omega_0^2}{3\pi^2 c \xi} \sin(2\omega_0 t) . \quad (146)$$

Here we made the approximation $\sin[2k_N^0 q(t)] - 2\xi \sin^2[k_N^0 q(t)] \simeq -2/(3\xi^3)$ with $k_N^0 q(t) \simeq n\pi + 1/\xi$. Notice that $P(t)$ tends to zero as ξ increases (that is, the reflectivity of the movable mirror tends to 1, see (142)).

Let P_{\max} be the maximum power entering the cavity. Then $|P(t)| \leq P_{\max}$ for all t and it follows from (146) that

$$g_0 \lesssim \sqrt{\xi \frac{3\pi^2 c}{\omega_0^2} \left(\frac{P_{\max}}{LW} \right)} . \quad (147)$$

If the maximum power is $P_{\max} = 1$ Watt, it follows from (138), (147), and the values of L and W above that

$$g_0 \lesssim 1.2 \times 10^{-6} \text{ N}^{1/2} \quad \text{if } \xi = 6.4 , \\ g_0 \lesssim 3.2 \times 10^{-6} \text{ N}^{1/2} \quad \text{if } \xi = 50 , \quad (148)$$

where g_0 is given in units of $\text{N}^{1/2}$.

Taking $g_0 \leq 10^{-6} \text{ N}^{-1/2}$ one gets from (139) the typical values $\Delta \leq 3.8 \times 10^6 \text{ 1/s}$ and $\Omega \geq 10^9$.

-
- [1] F. Marquardt and S. M. Girvin, *Physics* **2**, 40 (2009).
 - [2] D. Hunger, S. Camerer, M. Korppi, A. Jöckel, T. W. Hänsch, and P. Treutlein, *C. R. Physique* **12**, 871 (2011).
 - [3] M. C. Wu, O. Solgaard, and J. E. Ford, *J. Lightwave Technol.* **24**, 4433 (2006).
 - [4] M. Ludwig, B. Kubala, and F. Marquardt, *New Journal of Physics* **10**, 095013 (2008).
 - [5] J. Restrepo, J. Gabelli, C. Ciuti, and I. Favero, *C. R. Physique* **12**, 860 (2011).
 - [6] K. Borkje and S. M. Girvin, *New Journal of Physics* **14**, 085016 (2012).
 - [7] M. Abdi, A. R. Bahrampour, and D. Vitali, *Phys. Rev. A* **86**, 043803 (2012).
 - [8] J. Qian, A. A. Clerk, K. Hammerer, and F. Marquardt, *Phys. Rev. Lett.* **109**, 253601 (2012).
 - [9] G. Heinrich, J. G. E. Harris, and F. Marquardt, *Phys. Rev. A* **81**, 011801(R) (2010).
 - [10] M. Ludwig, A. H. Safavi-Naeini, O. Painter, and F. Marquardt, *Phys. Rev. Lett.* **109**, 063601 (2012).
 - [11] T. Carmon, H. Rokhsari, L. Yang, T. J. Kippenberg, and K. J. Vahala, *Phys. Rev. Lett.* **94**, 223902 (2005).
 - [12] T. J. Kippenberg, H. Rokhsari, T. Carmon, A. Scherer, and K. J. Vahala, *Phys. Rev. Lett.* **95**, 033901 (2005).
 - [13] F. Marquardt, J. G. E. Harris, and S. M. Girvin, *Phys. Rev. Lett.* **96**, 103901 (2006).
 - [14] C. Metzger, M. Ludwig, C. Neuenhahn, A. Ortlieb, I. Favero, K. Karrai, and F. Marquardt, *Phys. Rev. Lett.* **101**, 133903 (2008).
 - [15] F. Marino and F. Marin, *Phys. Rev. E* **83**, 015202(R) (2011).
 - [16] F. Marino and F. Marin, *Phys. Rev. E* **87**, 052906 (2013).
 - [17] S. Zaitsev, O. Gottlieb, and E. Buks, *Nonlinear Dyn.* **69**, 1589 (2012).
 - [18] S. Zaitsev, A. K. Pandey, O. Shtempluck, and E. Buks, *Phys. Rev. E* **84**, 046605 (2011).
 - [19] D. Blocher, R. H. Rand, A. T. Zehnder, *International Journal of Non-Linear Mechanics* **52**, 119 (1972).
 - [20] M. B. Spencer and W. E. Lamb Jr., *Phys. Rev. A* **5**, 884 (1972).
 - [21] R. Lang, M. O. Scully, and W. E. Lamb Jr., *Phys. Rev. A* **7**, 1788 (1973).
 - [22] B. Baseia and H. M. Nussenzweig, *Optica Acta: International Journal of Optics* **31**, 39 (1984).
 - [23] J. C. Penaforte and B. Baseia, *Phys. Rev. A* **30**, 1401 (1984).
 - [24] I. Guedes, J. C. Penaforte, and B. Baseia, *Phys. Rev. A* **40**, 2463 (1989).
 - [25] I. Guedes and B. Baseia, *Phys. Rev. A* **42**, 6858 (1990).
 - [26] S. M. Barnett and P. M. Radmore, *Opt. Commun.* **68**, 364 (1988).
 - [27] R. W. F. van der Plank and L. G. Suttorp, *Phys. Rev. A* **53**, 1791 (1996).
 - [28] S. M. Dutra, *Cavity Quantum Electrodynamics*, (Wiley, 2005).
 - [29] L. O. Castaños and R. Weder, *Equations of a moving mirror and the electromagnetic field*, to be published.
 - [30] M. Schwartz, *Principles of Electrodynamics*, (Dover Publications, 1987).
 - [31] L. Perko, *Non-linear systems and chaos*, 3rd edition, (Springer, 2001).
 - [32] R. A. Beaumont and R. S. Pierce, *The Algebraic Foundations of Mathematics*, (Addison-Wesley Pub. Co., 1963).
 - [33] R. L. Burden and J. D. Faires, *Numerical Analysis*, 7th edition, (Brooks/Cole, 2001).